Journal of African Earth Sciences 224 (2025) 105536

Contents lists available at ScienceDirect

Journal of African Earth Sciences

journal homepage: www.elsevier.com/locate/jafrearsci

# Provenance and source area weathering of sandstones from the Tarkwaian Group at the northeastern extent of the Paleoproterozoic Ashanti Belt, Ghana: Constraints from petrography and geochemistry

Victor Sedziafa [a,*], Ying Song [a,**], Emmanuel Daanoba Sunkari [b,c], Daniel Kwayisi [d,e], Chris Y. Anani [d], Daniel K. Asiedu [d]

[a] State Key Laboratory of Deep Oil and Gas, School of Geosciences, China University of Petroleum, P.O. Box 266580, East China, Qingdao, PR China
[b] Department of Geological Engineering, Faculty of Geosciences and Environmental Sciences, University of Mines and Technology, P. O. Box 237, Tarkwa, Ghana
[c] Department of Chemical Sciences, Faculty of Science, University of Johannesburg, P.O. Box 524, Auckland Park 2006, Johannesburg, South Africa
[d] Department of Earth Sciences, School of Physical and Mathematical Sciences, University of Ghana, P.O. Box LG 58, Legon, Accra, Ghana
[e] Department of Geology, Faculty of Science, University of Johannesburg, P.O. Box 524, Auckland Park 2006, Johannesburg, South Africa

ARTICLE INFO

Handling Editor: M Mapeo

*Keywords:*
Ashanti belt
Provenance
Sandstone
Tarkwaian group
Tectonic setting

ABSTRACT

An integrated geochemical and petrographic study was conducted on the Paleoproterozoic sandstones of the Tarkwaian Group exposed at the northeastern extent of the Ashanti Belt, Ghana. Recognizing the economic importance of the Tarkwaian Group, particularly owing to its extensive gold deposits, the primary objective was to investigate the provenance, tectonic setting, and crustal evolution of the Tarkwaian Group. The dominant quartz (polycrystalline and monocrystalline), together with minor muscovite, feldspar, hematite, and lithic fragments, characterize the sandstones and thus, the sandstones are classified as sublitharenite, and lithicsubarkose. Based on mineralogical composition and major element content, the sandstones can be classified as litharenite, sublitharenite, and minor greywacke. The high values of $SiO_2/Al_2O_3$ (average: 12.74), relatively moderate values of $K_2O/NaO_2$ (average: 1.42), and high quartz content (average: 88%) suggest that the sediments are compositionally sub-mature to mature. The sandstones likely underwent low to moderate levels of sedimentary sorting and recycling owing to angular to sub-rounded grains and moderate Zr/Sc and Th/Sc values. The high Chemical Index of Alteration (CIA) signature (average: 76.79 wt%), Plagioclase Index of Alteration (PIA) values (average: 90.13 wt%), and Index of Compositional Variability (ICV) (average: 0.61 wt%) suggest moderate to intense chemical weathering within the region of origin. Overall, the mineralogical and geochemical features of the sandstones, such as a high proportion of quartz and feldspar, and elevated concentrations of elements such as Zr, Sc and Th, and moderate to high ratios of $Al_2O_3/TiO_2$ and La/Sc indicate that they were likely sourced from felsic to intermediate igneous rocks and deposited in an active continental margin such as magmatic arc setting.

## 1. Introduction

Sedimentary rocks with significant silica content play a pivotal role in determining the origin, transport processes, tectonic setting, and paleoweathering of sediments, thereby offering critical insights into the paleoclimate and evolution of the continental crust (Nesbitt and Young, 1982; Suttner and Dutta, 1986; McLennan et al., 1993; Cullers, 2000; Kwayisi et al., 2022). The geochemical characteristics and detrital mineralogy of such sediments are fundamental for constraining their provenance (Nesbitt and Young, 1982; Dutta and Suttner, 1986; McLennan et al., 1993; Cullers, 2000).

Mineralogical and petrographic analyses of sandstones have been widely used to infer their provenance (Basu et al., 1975; Dickinson et al., 1983; Anani, 1999; Critelli et al., 2003; Marsaglia et al., 2016). Similarly, bulk-rock geochemical data have been instrumental in evaluating paleo-weathering conditions, provenance, and tectonic settings of source regions (McLennan et al., 1993; Kroonenberg, 1994; Verma and Armstrong-Altrin, 2013, 2016; Anani et al., 2017; Ghaznavi et al., 2018;

* Corresponding author.
** Corresponding author.
*E-mail addresses:* vsedziafa14@gmail.com (V. Sedziafa), yingsong@upc.edu.cn (Y. Song).

https://doi.org/10.1016/j.jafrearsci.2025.105536
Received 14 May 2024; Received in revised form 31 December 2024; Accepted 6 January 2025
Available online 9 January 2025

Jiang et al., 2019; Cullers, 2000; Asjad et al., 2021; Huang et al., 2022). These approaches are particularly valuable for studying Precambrian terranes, where the source regions are often eroded or their characteristics remain uncertain (Johnsson, 1993; Weltje and von Eynatten, 2004; Roddaz et al., 2007; Garzanti, 2019).

The West African Craton is predominantly composed of granitoid complexes that underwent deformation and metamorphism during the Eburnean orogeny around 2.1 Ga. These are associated with Paleoproterozoic greenstone belts and metasedimentary basins within the Birimian terrane (Fig. 1) (Sakyi et al., 2014, 2020; Nunoo et al., 2022). The Eburnean orogeny represents a significant event in juvenile crust formation in West Africa, with magmatic ages constrained to 2.1–2.2 Ga,

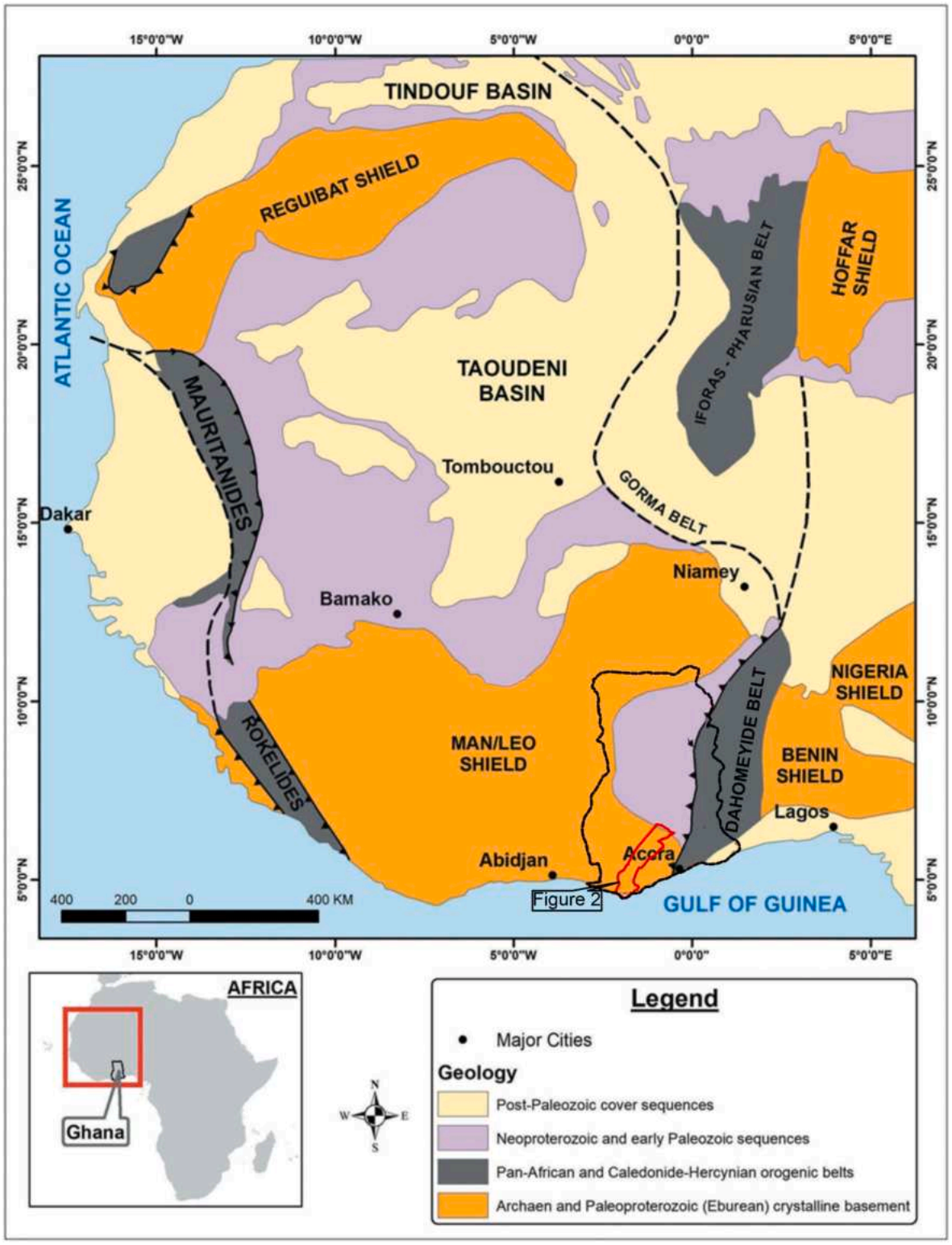


**Fig. 1.** Simplified geological map of the Man/Leo Shield of the West African Craton (WAC) indicating the position of Ghana modified after Carney et al. (2010). Inset showing a simplified map of Africa showing the position Ghana.

as revealed by precise U-Pb geochronology (Hirdes et al., 1992, 1996; Davis et al., 1994; Anum et al., 2015; Amponsah et al., 2023) and near-chondritic Nd and Hf isotopic signatures (Boher et al., 1992; Abouchami et al., 1990; Taylor et al., 1992).

In Ghana, the Paleoproterozoic Birimian Supergroup is characterized by six northeast-trending granitoid-greenstone belts interspersed with metasedimentary basins (Agra et al., 2023; Atanga et al., 2023; Kazapoe et al., 2023). Among these, the Ashanti Greenstone Belt is the principal gold-bearing belt within the Paleoproterozoic Birimian terrane of West Africa. This belt comprises volcano-sedimentary sequences intruded by granitoids dated between 2.2 and 2.1 Ga, and is renowned for its substantial gold resources (Hirdes et al., 1992; Oberthür et al., 1997; Dampare et al., 2009; Berge, 2011; Chudasama et al., 2016). The Tarkwaian Group, dated to less than 2132 Ma, occupies a synclinal basin within the Ashanti Belt and has been the focus of extensive research. Studies reveal that the Tarkwaian Group underwent folding and metamorphism under greenschist facies conditions associated with the Eburnean tectonothermal event around 2.1 Ga (Klemd et al., 2002; Chudasama et al., 2016).

The Tarkwaian Group, well known for hosting economically significant gold deposits ranging from alluvial to paleoplacer deposits, is thought to have formed in intermontane grabens, making it a major focal point for mineral exploration (Kesse, 1985; Leube and Hirdes, 1986). The Noyem-Nyafoman Gold Project (research area) located within the Tarkwaian Group in the northeastern Ashanti Belt, has drawn substantial academic interest due to the prevalence of small-scale mining operations in the area (Hirdes et al., 1996; Du Toit, 1996; Griffis et al., 2002). For example, Du Toit (1996) proposed a Phase 1 drilling program for the Noyem Gold Project aimed at mapping the stratigraphic and structural features of gold-bearing rocks, thereby providing a solid geological foundation for further exploration and resource estimation.

Field observations and U-Pb data indicate that the Tarkwaian Group rocks formed around 2132 Ma and may have received detrital inputs from the Paleoproterozoic Birimian terrain (Davis et al., 1993; Hirdes et al., 1996; Du Toit, 1996; Griffis et al., 2002; Fisher, 2019). Despite the significant efforts by these researchers, the tectonic setting, provenance, and crustal evolution of the Tarkwaian Group at the northeastern extent of the Ashanti Belt remain understudied, especially through petrographic and geochemical analysis of its clastic sedimentary rocks.

Sedimentary rocks are widely regarded as essential for studying crustal evolution, as their petrographic characteristics and geochemical signatures offer valuable information about provenance, source area weathering, paleoclimate, tectonic settings, and the identification of economically significant mineral deposits (Nesbitt and Young, 1982; Bhatia and Crook, 1986; Verma and Armstrong-Altrin, 2016). However, debates persist regarding the origins of these Tarkwaian sediments, specifically whether their sources are exclusively linked to the Paleoproterozoic Birimian terrane or whether external contributions also played a role (Davis et al., 1994; Koffi et al., 2016; Wilson et al., 2022).

Given these uncertainties, this study investigates the geochemistry and petrography of sandstones within the Noyem-Nyafoman Gold Project area to clarify their provenance (i.e., from the Paleoproterozoic Birimian terrain or alternative sources) and tectonic setting (passive or active margin). The findings from these analyses can be employed to investigate the tectonic setting and provenance of sandstones, which can provide valuable insights into the tectonic and sedimentary evolution of the region. Such knowledge could further inform and enhance mineral exploration initiatives within the Birimian and Tarkwaian terranes of Ghana.

Petrographic and geochemical analyses are valuable tools for elucidating the provenance and tectonic setting of sandstones (Verma and Armstrong-Altrin, 2016), and incorporating zircon U-Pb geochronology alongside Lu-Hf isotopic data provides an opportunity for greater precision. This integrated approach could enhance the findings and offer deeper insights into the geological evolution and significance of the Tarkwaian Group within the regional context (Anani et al., 2020). Other limitations may affect the generalizability and scope of the conclusions of this study. For example, the sampling was confined to the Noyem-Nyafoman area within the Tarkwaian Group, which may not fully capture the regional sedimentary and tectonic variability across the broader Ashanti Belt.

Additionally, results may be less applicable beyond the Paleoproterozoic terranes due to the geological differences, and post-depositional alterations, which may introduce further uncertainties that could influence interpretations of crustal evolution and sedimentary history. Nonetheless, this petrographic and geochemical investigation represents a critical initial step toward understanding the provenance and tectonic setting of the Tarkwaian Group sandstones.

## 2. Geological setting

The Noyem-Nyafoman Gold Exploration Project (the study area, is located on the northeastern margin of Ghana's Ashanti Belt. This region is primarily composed of clastic metasedimentary rocks belonging to the Tarkwaian Group (Fig. 2). The study area is predominantly underlain by meta-volcano-sedimentary sequences of Paleoproterozoic rocks associated with the Birimian terrane as well as siliciclastic formations of the Tarkwaian Group. The Birimian terrane is characterized by narrow, northeast-trending greenstone belts ranging from 20 to 60 km in width, which have undergone metamorphism predominantly under greenschist facies conditions (Griffis et al., 2002; Smith et al., 2016; Nunoo et al., 2022). Deformation, including brittle faulting and ductile folding, is common in the Birimian terrane. These deformations have been postulated to coincide with the peak temperature-pressure of metamorphism during Eburnean thermo-tectonic events at approximately 2100 Ma (Hirdes et al., 1996; Griffis et al., 2002). The mineralization of gold in the Birimian terrane primarily occurs in structurally controlled lithologies (Sunkari et al., 2024a). These are mesothermal vein-hosted deposits, with most Birimian-aged mesothermal gold deposits found near Obuasi Town (Griffis et al., 2002). Overlying the Birimian terrane is a distinctive sedimentary sequence of rocks known as the Tarkwaian Group, which is exposed in the northeast-trending Bui and Ashanti Belts (Griffis et al., 2002; Leaders et al., 2018).

However, the Tarkwaian Group is predominantly composed of a variety of sandstones, phyllites, indurated clay particles, and conglomerates (Griffis et al., 2002; Pigois et al., 2003; Sunkari et al., 2024b). Four stratigraphic successions were identified within the Tarkwaian Group (Table 1). These successions, listed from bottom to top, include the Kawere Sandstones, Banket Conglomerate, Tarkwa Phyllite, and Huni Sandstones (Kesse, 1985). The Kawere unit consists of sandstones and minor conglomerates with thicknesses ranging from 250 to 700 m. The overlying Banket Series consists of conglomerates featuring Birimian quartz pebbles and volcanic clasts, along with interbedded cross-bedded sandstones. The Banket Series holds the <100 m thick gold zone of the Tarkwa Placer gold deposit, which reaches an estimated maximum thickness of 600 m and is overlain by the Tarkwa Phyllite, of up to 400 m thick. The latter was subsequently covered by the topmost Huni Sandstone, which is composed of a series of sandstones that are about 1370 m thick and are occasionally interrupted by small dolerite sills (Kesse, 1985; Griffis et al., 2002; Pigois et al., 2003; Perrouty et al., 2012).

Conglomeratic units (Banket Series) from the Tarkwaian Group are considered to have undergone reworking after being deposited in alluvial fans due to braided stream channels (Sestini, 1973; Griffis et al., 2002). Based on detrital zircons from the Banket Series and Kawere sandstones, the maximum deposition age for the Tarkwaian Group was limited to approximately 2133–2132 Ma (Davis et al., 1994; Pigois et al., 2003; Perrouty et al., 2012). However, some estimates suggest that deposition could have started as late as 2107 Ma. Additionally, the intrusion of meta-gabbro sills and granitoids constrains the deposition age within the Tarkwaian Group to approximately 2102 to 2097 Ma (Adadey et al., 2009). Mineralization of gold in the Tarkwaian Group

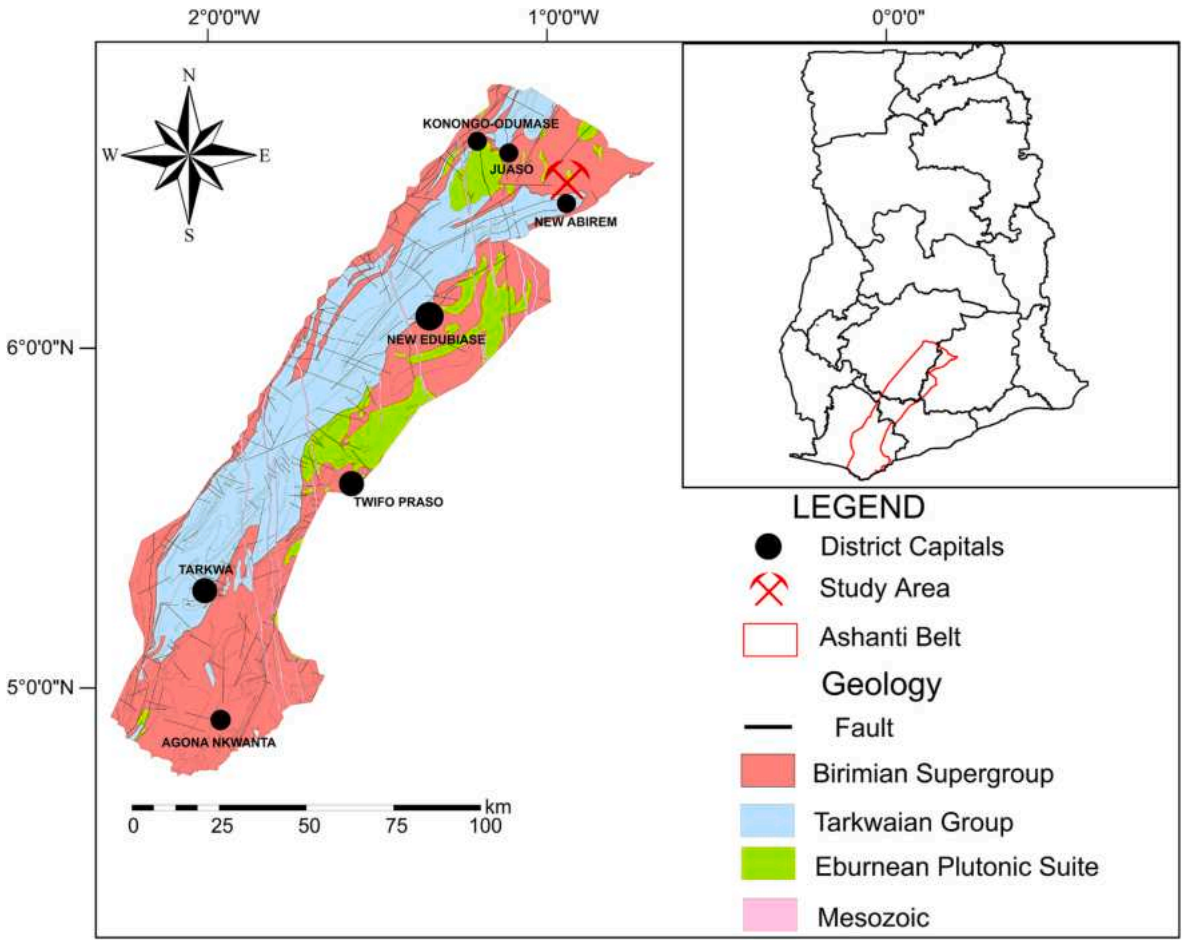


**Fig. 2.** Simplified geological map of the Ashanti Belt. The insert map illustrates the simplified map of Ghana indicating the position of the Ashanti Belt.

**Table 1**
Summarized stratigraphy of the Tarkwaian Group (Modified after Kesse, 1985).

| GROUP | SERIES | THICKNESS (m) | LITHOLOGY |
|---|---|---|---|
| **Tarkwaian** | Huni Sandstone | 1370 | Sandstones, minor phyllite |
| | Tarkwa Phyllite | 120–400 | Chloritic and sericitic phyllite, and schists |
| | Banket Series | 120–600 | Quartzites, coarse sandstone and conglomerates |
| | Kawere Conglomerates | 250–700 | Quartzites, coarse sandstone and conglomerates |
| **Major Unconformity** | | | |
| **Birimian Super Group** | Birimian | | Meta-volcanics, volcaniclastics and sediments |

occurs primarily within sedimentologically controlled, palaeoplacer conglomerate-hosted deposits, with the majority of the Tarkwaian-aged palaeoplacer gold deposits discovered within the Tarkwa area (Griffis et al., 2002). In contrast, the mineralization of gold in the Birimian terrane occurs primarily within structurally controlled lithologies, and mesothermal vein-hosted deposits (Griffis et al., 2002; Sunkari et al., 2024a).

In summary, the geological settings of the study area located in the northeastern Ashanti Belt of Ghana feature a synclinal structure with Paleoproterozoic Birimian meta-volcano-sedimentary sequences and Tarkwaian siliciclastic rocks. The Birimian terrane includes northeast-trending greenstone belts and metasedimentary basins at greenschist facies metamorphism with the Tarkwaian Group comprising sedimentary and gold-bearing units that were significantly deformed and metamorphosed during the Eburnean orogeny (~2.1 Ga), reflecting diverse tectonic environments from the passive margins.

## 3. Sampling and Analytical techniques

### 3.1. Sampling

Sandstone samples were collected from active artisanal mining pits within the Noyem-Nyafoman gold project area. A total of 25 least-weathered samples, comprising 15 quartzitic and 10 feldspathic sandstone samples, were selected for petrographic and geochemical analyses.

### 3.2. Petrographic analysis

Using the Gazzi-Dickinson approach (Dickinson, 1970; Ingersoll et al., 1984), modal analysis of framework grains was carried out by point-counting, with 500 points tallied for each thin slice at the Department of Earth Science, University of Ghana.

### 3.3. Geochemical analysis

The whole-rock geochemical analysis of the samples followed standard preparatory techniques. After the samples were weighed, dried, and registered in the tracking system, they were finely crushed to 70% $< 2$ mm. A portion of 250 g was then separated and pulverized to achieve a particle size of more than 85%, passing 75 μm at the ALS laboratory in Vancouver, Canada. The major elements were analyzed using

inductively coupled plasma atomic emission spectroscopy (ICP-AES). Approximately 0.200 g of the prepared sample was fused with lithium metaborate in a furnace at 1025 °C. Subsequently, the melt was allowed to cool and dissolved in an acid combination of hydrochloric (HCl), hydrofluoric (HF), and nitric ($HNO_3$) acids, and its principal element composition was examined using ICP-AES, which has a precision of better than 5%. The base metals were also analyzed using ICP-AES. A mixture of perchloric ($HClO_4$), $HNO_3$, HCl, and HF acids was used to digest a 0.25g prepared sample. ICP-AES was used to evaluate the residue with an accuracy of greater than 7% after it had been digested and diluted with diluted HCl with results corrected for spectral inter element interferences. For the trace element analysis, inductively coupled plasma-mass spectroscopy (ICP-MS) was used with a precision of better than 7%. This involved lithium borate fusion of a prepared sample weighing 0.100 g and acid digestion in a mixture of $HNO_3$, HCl, and HF. Fig. 3 illustrates a summary of the methodologies adopted in this study.

## 4. Results

### 4.1. Field relations

Fig. 4a, located at coordinates 6°25′54″ N, 0°56′36″ E, depicts a medium-to coarse-grained sandstone characterized by poor sorting and a mixture of quartz and feldspar. It contains angular to sub angular grains, indicating minimal transport and possible proximal deposition from the source area. This characteristic is typical of fluvial deposits in the Tarkwaian (Leube et al., 1990; Griffis et al., 2002). The presence of mudstone intraclasts suggests episodic, high-energy events. Heterogeneity in the grain size and composition of the sample indicates varying depositional conditions. These geological features can be useful for reconstructing the sedimentary processes.

Fig. 4b with coordinates: 6°26′12″ N, 0°56′41″ E depicts a medium-grained sandstone with sub-rounded to sub-angular quartz and feldspar grains. It shows evidence of cross-bedding and ripple marks, indicating deposition in a high-energy shallow marine environment. The presence of iron-oxide staining suggests significant post-depositional weathering. The presence of quartz and minor feldspar indicates more mature sediment, which is characteristic of the braided river systems of the Tarkwaian (Yadav et al., 2022). This sample is crucial for understanding the sedimentary processes and diagenetic alterations.

Fig. 4c, with coordinates of 6°27′13″ N, 0°55′42″ E, features poorly sorted conglomeratic sandstone, coarse pebbles, and cobbles within a sandy matrix. The clasts are sub-angular to sub-rounded, indicating a high-energy depositional environment likely proximal to the source within an alluvial fan system. These features provide important information for understanding the sedimentary basin dynamics and provenance (Afify et al., 2023).

Fig. 4d shows the coordinates of 6°27′14″ N, 0°55′45″ E, which is a coarse-grained, quartz-rich sandstone with well-rounded grains. The high quartz content and grain rounding suggest the occurrence of significant weathering and transport. This composition is characteristic of mature fluvial deposits in the Tarkwaian. This sample is key to understanding the dynamics of sediment transport and depositional processes in ancient river systems (Makulana et al., 2022).

### 4.2. Petrography

All twenty-five (25) thin sections of the samples were carefully subjected to quantitative and descriptive analyses using a Leica DM750P polarizing microscope at the Petrographical Laboratory of the Earth Science Department, University of Ghana. The studied sandstones comprise fine-to medium sand-sized grains that are moderately sorted and sub-rounded to rounded. Sandstones from the Noyem-Nyafoman Gold Project (which can be associated with the Banket Series) are mainly comprised of quartz, feldspar, muscovite, and hematite (Fig. 5 a-h). A modal study of the studied sandstones revealed a predominant quartz content ranging from 61.5 to 77.3%, as indicated in Table 2. Monocrystalline quartz (Qm) dominated polycrystalline quartz (Qp) (Fig. 5a and b). Muscovite grains appear to be shredded between the quartz grains, whereas feldspars are weathered into sericites (Fig. 5). Some thin sections showed quartz grains and shredded muscovite minerals aligned in a preferred planar orientation.

### 4.3. Geochemistry

The presence of major elements reflects the mineralogical composition of the rocks (Armstrong-Altrin et al., 2018; Brako et al., 2022). The Appendix table shows the variable quantities of the main oxides for the twenty (25) selected sandstone samples, which varied in the following order: $SiO_2$ (74.70–94.70) wt.%, $Al_2O_3$ (2.71–12.75) wt.%, MgO (0.03–0.15 wt%), $Na_2O$ (0.28–1.47) wt.%, CaO (0.01–0.14) wt.% $K_2O$ (0.38–1.77) wt.%, $TiO_2$ (0.09–0.82 wt%), MnO (0.01–0.10) wt.%. In the Harker plots (Fig. 6), there is a good correlation between the major oxides and $SiO_2$, except for $P_2O_5$ and CaO, which showed no preferred correlation. The sandstones from the Noyem-Nyafoman gold project area have mineralogical and major element compositions typical of litharenite, subarkose, and sublitharenite (Fig. 7a and b). The Noyem-Nyafoman sandstones exhibit relatively high REEs compared to chondrites, defining an enriched LREE pattern relative to both the MREE and HREE, with the MREE and HREE showing a flat pattern (Fig. 12a). The REE pattern for the sandstones from the Noyem-Nyafoman gold project area is comparable to that of UCC and PAAS (Fig. 12a). All samples exhibited a positive Eu/Eu* anomaly ranging from 0.79 0.96 (Appendix). After normalizing the multi-element graphic to the UCC, the

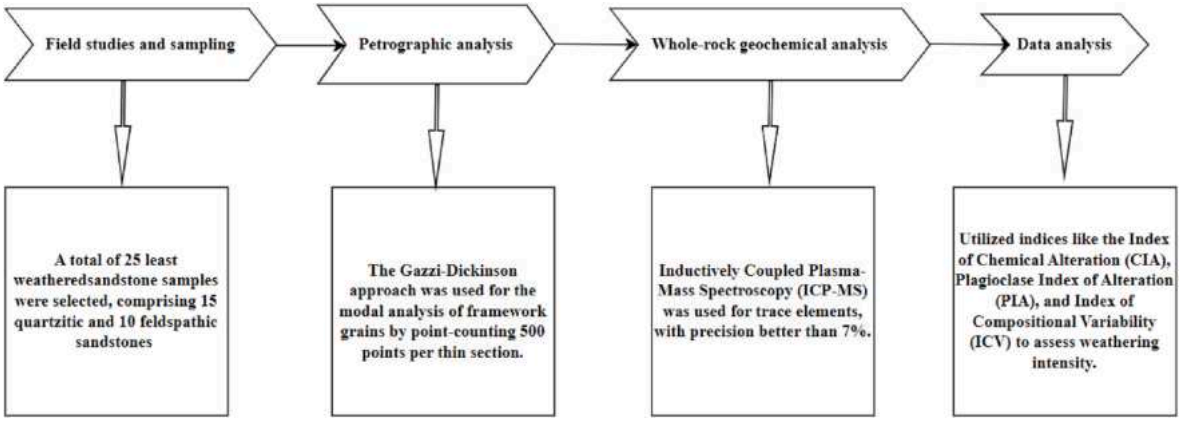


**Fig. 3.** Flowchart summarizing the methods used in the research.


**Fig. 4.** Field photos of sandstones obtained from the Tarkwaian at the northeastern extent of the Ashanti belt, Ghana.

Noyem-Nyafoman sandstones displayed slight LILE depletion compared to HFS, UCC, and PAAS (Fig. 12b). They exhibit negative peaks for Ti, Ta, Nb, and P.

## 5. Discussion

### 5.1. Sediment maturity and recycling

Textural attributes, including grain size, grain shape, and mineralogical composition, are essential parameters for evaluating the maturity and sorting of siliciclastic sedimentary rocks (McLennan et al., 1993; Akarish and El-Gohary, 2008). The Noyem-Nyafoman sandstones exhibit moderate quartz content, with angular to sub-rounded grains, along with sericite and muscovite. These characteristics indicated that the sediments were moderately sorted and displayed a moderate level of maturity. These observations indicate significant weathering and transport, with the presence of hematite, indicating potential sedimentary recycling. These characteristics reflect advanced, although not extreme, maturity, aligning with recent research on sedimentary rock evolution and diagenetic processes (Johnsson, 1993; Weltje and von Eynatten, 2004; Garzanti and Andò, 2018). High textural maturity, characterized by well-sorted and rounded grains, does not always signify extended transport or prolonged weathering. Instead, sediment maturity may be strongly influenced by the depositional environment and the nature of the source rock (Garzanti, 2017). Furthermore, elevated textural maturity does not necessarily correspond to an advanced diagenetic history; instead, it may arise from immediate depositional processes or the initial fragmentation properties of the source material (Garzanti, 2019). Additionally, the $SiO_2/Al_2O_3$ ratio is widely recognized as a robust metric for assessing sediment maturity (Cullers, 1994; Hadji et al., 2024).

The $SiO_2/Al_2O_3$ ratio is widely used to evaluate the textural maturity of rocks containing clastic sediments, with higher values (>10) typically indicating a higher degree of sediment maturity (Armstrong-Altrin et al., 2015; Abu and Sunkari, 2020a). In the Noyem-Nyafoman Gold Project area, the sandstones exhibited $SiO_2/Al_2O_3$ ratios ranging from 12.7 to 94.7 (Table 3), suggesting that these sediments range from moderately mature to mature (Abu and Sunkari, 2020b).

The concentrations of $Na_2O$ and $K_2O$ provided insights into the feldspar content and degree of chemical weathering. Higher $K_2O$ values typically indicate less weathered, texturally immature sediments with limited recycling, whereas lower values suggest advanced weathering and sedimentary recycling (Nesbitt and Young, 1984; McLennan and Taylor, 1991; Cullers, 1994). In the case of the Noyem-Nyafoman sandstones, $K_2O$ content ranges from 0.38 to 1.77 wt%, reflecting significant weathering of the source material and indicating sedimentary maturity with extensive recycling. The $Na_2O$ content in the studied sandstone samples ranges from 0.28 to 1.47 wt%, reflecting variability in sedimentary maturity and the extent of recycling within the formation. Lower $Na_2O$ values are indicative of greater sedimentary maturity and more extensive recycling, as sodium is readily leached during chemical weathering. This suggests pronounced weathering and the removal of less stable minerals from the source material (Nesbitt and Young, 1982; Cullers, 1994).

The $TiO_2$ (0.09–0.82 wt%) and MnO (0.01–0.10 wt%) concentrations in the analyzed sandstones indicate the presence of stable heavy minerals and suggest oxidative depositional conditions. The low MnO values, combined with the variability in $TiO_2$, reflect a high degree of sedimentary maturity and extensive recycling, where less stable minerals are removed, leaving more resistant phases behind (McLennan and Taylor, 1991). Additionally, the low MnO content (0.01–0.10 wt%) is consistent with extensive weathering and recycling, further emphasizing the mature nature of these sediments (McLennan and Taylor, 1991; Cullers, 1994).

The Index of Compositional Variability (ICV) is a geochemical parameter commonly used to evaluate the maturity of siliciclastic sedimentary rocks. It is calculated using the formula: $ICV = (Al_2O_3 + K_2O + Na_2O + CaO + MgO + TiO_2)/Al_2O_3$ (Cox et al., 1995).

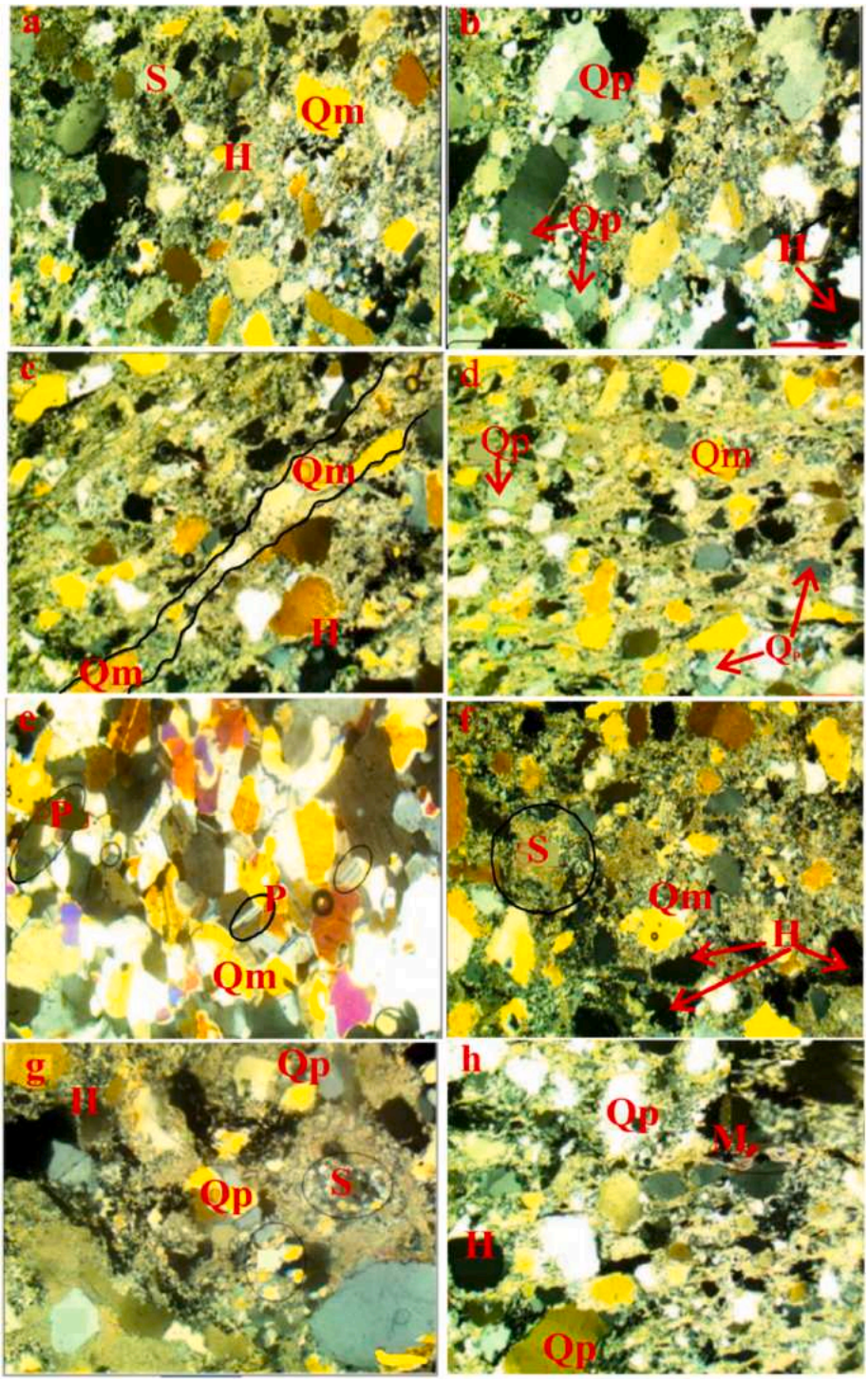


**Fig. 5.** Photomicrographs of the studied sandstones from Noyem-Nyafoman under crossed polarized light (Qm = monocrystalline quartz, Qp. = polycrystalline quartz, Op = opaque minerals, S = sericite, H = hematite, M = muscovite, P = plagioclase (All scale bars are 0.2 mm).

Geochemically mature siliciclastic rocks are typically characterized by ICV values below 1, whereas immature, first-cycle sediments generally display ICV values greater than 1 (Cox et al., 1995).

The sandstones from the study area display ICV values below 1 (Table 4), signifying a relatively advanced level of chemical maturity. Suttner and Dutta (1986) proposed a bivariate plot of $SiO_2$ versus ($Al_2O_3$ + $K_2O$ + $Na_2O$) as a valuable tool for evaluating the chemical maturity of siliciclastic sedimentary rocks (Fig. 7a). The Noyem-Nyafoman sandstones exhibit increasing chemical maturity, which may reflect a progressive evolution of sedimentary processes toward greater maturity. The observed variations across different climatic zones likely highlight the impact of environmental factors on sediment composition (Suttner and Dutta, 1986). This is reflected in the elevated $SiO_2/Al_2O_3$ ratios and higher quartz content, which signify the removal of less stable minerals through weathering and sedimentary recycling, resulting in a more compositionally mature sediment (Garzanti, 2017, 2019).

Research indicates that $K_2O$ typically constitutes 5–10% of the total weight in most illite mineral compositions (Panahi and Young, 1997). This suggests that sedimentary rocks derived from reworked or recycled sources may show $K_2O$ enrichment. For the studied sandstones, the

**Table 2**
Detrital modes of quartzites from Noyem-Nyafoman sandstones (vol. %). L = H + M, F=P + S, Lt = $Q_p$ + M + H(L + $Q_p$) Lithic fragments Q = quartz, F = total feldspars H = hematite, M = Muscovite S = sericite Qm = monocrystalline quartz, Qp = polycrystalline, Lt = total lithic fragments (after Dickinson, 1985).

| | | | | | | | QFL% | | | QmFLt (%) | | |
|---|---|---|---|---|---|---|---|---|---|---|---|---|
| Sample | Qm | Qp | P | H | S | M | L | F | Q | Lt | F | Qm |
| P1B | 66.2 | 4.4 | 5.1 | 17.3 | 4.7 | 2.3 | 19.6 | 9.8 | 70.6 | 24.0 | 9.8 | 66.2 |
| P1C | 65.9 | 3.2 | 8.3 | 10.2 | 8.2 | 4.2 | 14.4 | 16.5 | 69.1 | 17.6 | 16.5 | 65.9 |
| P1D | 68.7 | 3.8 | 8.6 | 11.5 | 2.7 | 4.7 | 16.2 | 11.3 | 72.5 | 20.0 | 11.3 | 68.7 |
| P1E | 69.8 | 2.9 | 5.8 | 12.8 | 3.5 | 5.2 | 18.0 | 9.3 | 72.7 | 20.9 | 9.3 | 69.8 |
| P1F | 65.5 | 5.4 | 6.2 | 15.0 | 6.2 | 1.7 | 16.7 | 12.4 | 70.9 | 22.1 | 12.4 | 65.5 |
| P1G | 68.3 | 0.0 | 0.0 | 15.9 | 9.6 | 6.2 | 22.1 | 9.6 | 68.3 | 22.1 | 9.6 | 68.3 |
| P1H | 62.5 | 4.8 | 5.5 | 18.2 | 3.8 | 5.2 | 23.4 | 9.3 | 67.3 | 28.2 | 9.3 | 62.5 |
| P1J | 76.0 | 1.3 | 6.3 | 11.5 | 2.1 | 2.8 | 14.3 | 8.4 | 77.3 | 15.6 | 8.4 | 76.0 |
| P2C | 74.9 | 0.0 | 0.0 | 10.7 | 9.6 | 4.8 | 15.5 | 9.6 | 74.9 | 15.6 | 9.6 | 74.9 |
| P1K | 63.0 | 3.8 | 7.8 | 15.5 | 5.6 | 4.3 | 19.8 | 13.4 | 66.8 | 23.6 | 13.4 | 63.0 |
| P1O | 60.0 | 4.1 | 9.3 | 13.2 | 8.8 | 4.6 | 17.8 | 18.1 | 64.1 | 21.9 | 18.1 | 60.0 |
| P1N | 65.1 | 3.9 | 7.8 | 12.0 | 8.6 | 2.6 | 14.6 | 16.4 | 69.0 | 18.5 | 16.4 | 65.1 |
| P1M | 71.5 | 1.8 | 6.6 | 16.1 | 2.2 | 1.8 | 17.9 | 8.8 | 73.3 | 19.7 | 8.8 | 71.5 |
| P1P | 73.6 | 0.0 | 0.0 | 12.0 | 9.5 | 4.9 | 16.9 | 9.5 | 73.6 | 16.9 | 9.5 | 73.6 |
| P1R | 64.8 | 0.0 | 0.0 | 20.1 | 9.3 | 5.8 | 25.9 | 9.3 | 64.8 | 25.9 | 9.3 | 64.8 |
| P2U | 67.3 | 2.7 | 4.8 | 12.9 | 5.6 | 6.7 | 19.6 | 10.4 | 70.0 | 22.3 | 10.4 | 67.3 |
| P2A | 73.3 | 0.0 | 0.0 | 12.0 | 9.2 | 5.5 | 17.5 | 9.2 | 73.3 | 17.5 | 9.2 | 73.3 |
| P2S | 71.0 | 0.0 | 0.0 | 14.6 | 9.7 | 4.7 | 19.3 | 9.7 | 71.0 | 19.3 | 9.7 | 71.0 |
| P3A | 63.6 | 4.8 | 7.7 | 10.8 | 9.7 | 3.4 | 14.2 | 17.4 | 68.4 | 19.0 | 17.4 | 63.6 |
| P3B | 61.3 | 6.3 | 7.4 | 12.6 | 8.2 | 4.2 | 16.8 | 15.6 | 67.6 | 23.1 | 15.6 | 61.3 |
| P3C | 68.1 | 1.6 | 8.1 | 15.6 | 2.1 | 4.5 | 20.1 | 10.2 | 69.7 | 21.7 | 10.2 | 68.1 |
| P3D | 64.3 | 3.8 | 8.8 | 12.5 | 6.8 | 3.8 | 19.3 | 15.6 | 68.1 | 23.1 | 15.6 | 64.3 |
| P3E | 62.6 | 4.4 | 9.4 | 10.4 | 9.8 | 3.4 | 13.8 | 19.2 | 67.0 | 18.2 | 19.2 | 62.6 |
| P3F | 56.2 | 5.3 | 8.6 | 15.5 | 9.2 | 5.2 | 20.7 | 17.8 | 61.5 | 26.0 | 17.8 | 56.2 |
| P3K | 71.9 | 1.2 | 7.3 | 12.2 | 1.9 | 5.5 | 17.7 | 9.2 | 73.1 | 18.9 | 9.2 | 71.9 |

$K_2O/Al_2O_3$ ratios range from 0.12 to 0.22, with an average value of 0.14.

This ratio falls within the typical range for sedimentary rocks, reflecting the presence of recycled illite-rich mudrock components and indicating that these sandstones have undergone sedimentary recycling to some extent. Features such as inherited quartz overgrowths, angular to sub-rounded grain shapes, and a higher proportion of quartz relative to other minerals are indicative of varying degrees of sedimentary recycling (Sen and Mishra, 2023). Additionally, the use of Th/Sc versus Zr/Sc plots has been extensively documented as an effective approach for evaluating the relationship between Zr enrichment and sedimentary recycling (McLennan et al., 1993).

The Zr/Sc and Th/Sc ratios are reliable indicators of provenance, as Sc is significantly enriched in Zr-bearing minerals (McLennan et al., 1990). Variations in these ratios provide valuable insights into sediment recycling and sorting processes. The Th/Sc ratios of the analyzed sandstones range from 0.24 to 0.82, suggesting a provenance derived from mature or recycled sedimentary source rocks. This observation aligns with the established relationship between Th/Sc ratios and sedimentary recycling, where Th/Sc values typically increase with progressive weathering and recycling of the parent rocks.

The Noyem-Nyafoman sandstones exhibit a trend towards sediment recycling on the Zr/Sc versus Th/Sc plot (Fig. 7b). This trend, marked by Zr enrichment, reflects the incorporation of zircon and sedimentary sorting processes. The data suggest that the sediments likely originated from moderately recycled sources comprising a mixture of felsic and intermediate compositions or were derived from diverse sources, including igneous, metamorphic, and older sedimentary rocks. Additionally, negative anomalies in Nb, Ta, P, and Ti within the sandstones may further indicate sedimentary maturity and recycling. The depletion of Nb and Ta, which are generally immobile during weathering, highlights intense chemical weathering and recycling processes, pointing to a mature sedimentary source (Nesbitt and Young, 1982).

The enrichment of titanium (Ti), niobium (Nb), and yttrium (Y) in the analyzed sandstones indicates a high degree of sedimentary maturity and significant recycling. The stability of Ti reflects prolonged weathering and transport processes, while Nb enrichment suggests a source dominated by resistant minerals. Similarly, Y, commonly associated with heavy minerals, highlights the role of sediment sorting and recycling. These elements are considered reliable indicators of sediment provenance and diagenetic history due to their resistance to alteration during weathering (Nesbitt and Young, 1982).

The Ti concentrations in the sandstones range from 0.09 to 0.82 wt%, while Y values span from 6.70 to 33.90 ppm. These values, as suggested by Nesbitt and Young (1982) and McLennan et al. (1990), signify advanced sedimentary maturity and extensive recycling of parent materials. The enrichment of refractory elements like Ti and heavy rare earth elements such as Y aligns with the processes of weathering and recycling observed in the Tarkwaian sandstones. These geochemical attributes provide critical insights into the provenance and tectonic setting of the studied sediments.

### 5.2. *Provenance, source rock composition and source area weathering*

The mineralogical and chemical characteristics of silica-rich sedimentary rocks are intricately linked to the attributes of their source rocks. Factors such as weathering intensity, transportation processes, climatic conditions, and topographical relief play pivotal roles in shaping the composition of parent rocks, subsequently influencing the chemical and mineralogical properties of siliciclastic sedimentary rocks (Armstrong-Altrin et al., 2015, 2017; McLennan et al., 1990; Anani et al., 2017). High quartz content in sandstones is particularly significant, as it provides valuable insights into the weathering processes in the source region (Pettijohn et al., 1987). In the Noyem-Nyafoman sandstone, quartz constitutes approximately 61.5–77.3% of the modal composition (Table 2), underscoring its implications for the sediment's provenance and weathering history.

The QFL ternary diagram is widely employed to interpret source area weathering conditions and sediment provenance (Suttner et al., 1981). As illustrated in Fig. 8a, the analyzed sandstone samples from the study area predominantly plot within the sublitharenite and lithicsubarkose fields of the QFL diagram. This distribution indicates a provenance characterized by moderate degrees of weathering and reworking of the source rocks prior to deposition (Dickinson, 1970; Weltje, 1994; Fedo et al., 1996). The presence of feldspar and lithic fragments highlights limited removal of less stable minerals, such as feldspars and rock fragments, through weathering and sedimentary recycling processes.

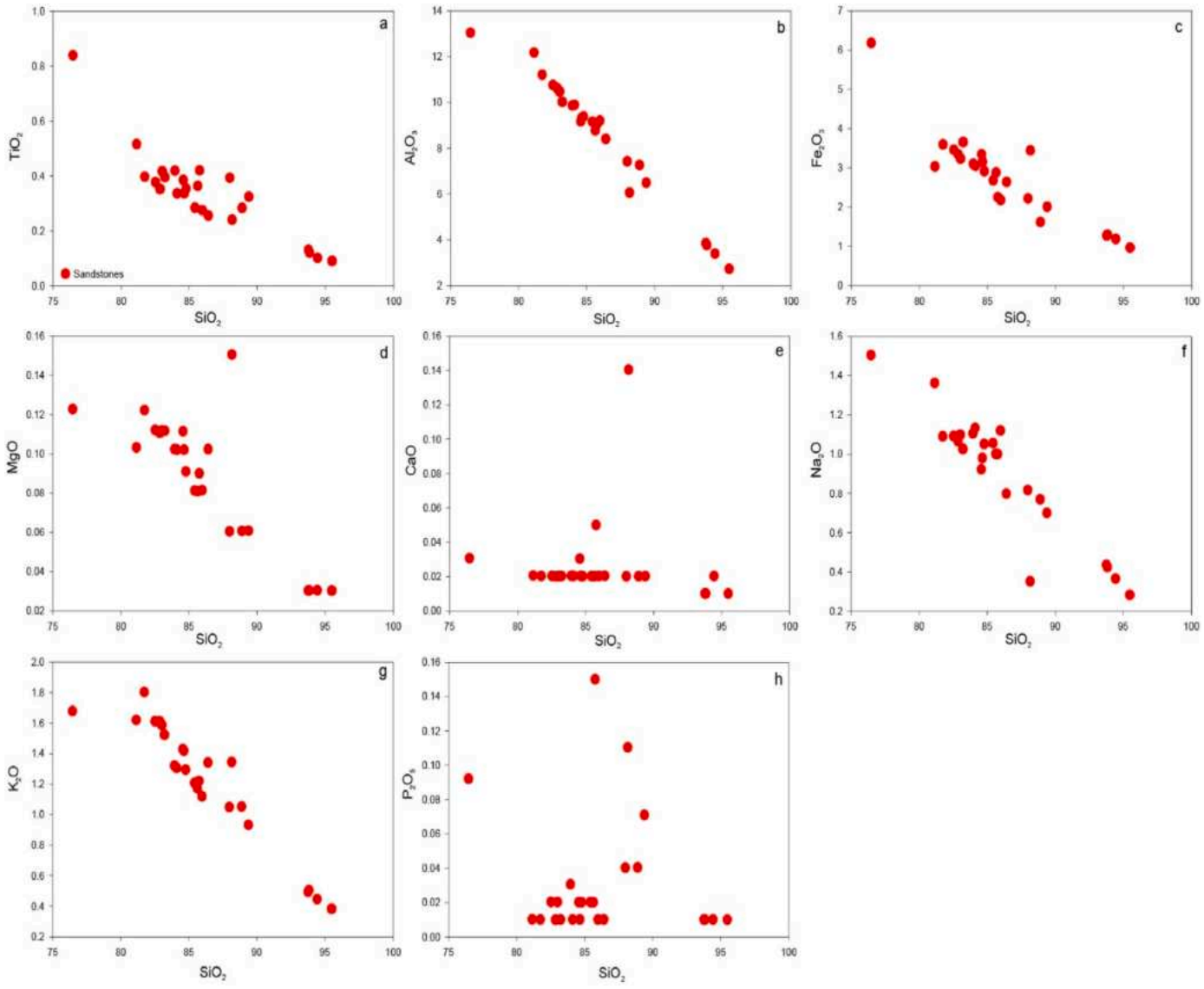


**Fig. 6.** Harker diagrams showing major oxide variations with silica for the studied sandstones.

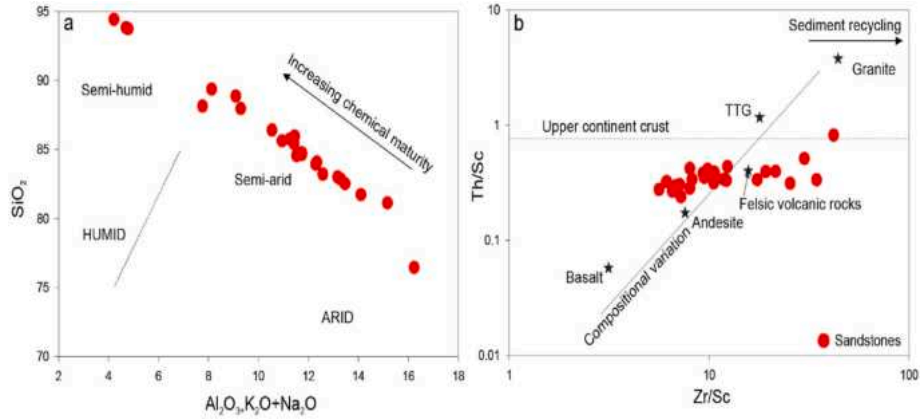


**Fig. 7.** (a) Bivariate plot of $SiO_2$ versus $Al_2O_3$+ $K_2O$ + $Na_2O$ of the studied sandstones from the Tarkwaian Group, from the Northeastern extent of the Ashanti Belt, Ghana (after Suttner and Dutta (1986) (b) Plots of Th/Sc versus Zr/Sc for the studied sandstones from Tarkwaian Group at the Northeastern extent of Ashanti Belt, Ghana (after McLennan et al., 1993).

**Table 3**
Geochemical characteristics of sediments derived from different provenance types (after McLennan et al., 1993; Girty et al., 1996).

| Sample | Th/U | Zr/Sc | Th/Sc | CIA | ICV | CIW | PIA | Sm N | Eu N | Gd N | Eu/Eu* |
|---|---|---|---|---|---|---|---|---|---|---|---|
| P1B | 1.55 | 11.81 | 0.34 | 79.93 | 0.56 | 89.59 | 124.34 | 150.26 | 81.90 | 66.22 | 0.82 |
| P1D | 1.10 | 21.50 | 0.40 | 80.34 | 0.64 | 89.81 | 44.80 | 9.64 | 6.53 | 6.29 | 0.84 |
| P1F | 0.91 | 34.50 | 0.34 | 80.18 | 0.65 | 90.33 | 39.31 | 9.44 | 7.35 | 6.22 | 0.96 |
| P1J | 1.60 | 12.20 | 0.33 | 79.78 | 0.53 | 90.20 | 107.91 | 34.67 | 20.27 | 16.72 | 0.84 |
| P1K | 1.42 | 29.91 | 0.51 | 79.74 | 0.62 | 89.87 | 107.05 | 38.72 | 22.72 | 18.73 | 0.84 |
| P1O | 1.08 | 25.40 | 0.31 | 80.04 | 0.64 | 89.66 | 50.96 | 8.67 | 6.67 | 6.18 | 0.91 |
| P3K | 3.62 | 9.29 | 0.38 | 76.75 | 0.94 | 92.50 | 155.95 | 6.72 | 5.17 | 5.37 | 0.86 |
| P1M | 1.57 | 19.20 | 0.40 | 79.70 | 0.64 | 90.01 | 95.12 | 52.31 | 30.20 | 24.75 | 0.84 |
| P1R | 1.14 | 17.40 | 0.34 | 80.38 | 0.62 | 89.65 | 49.65 | 9.38 | 6.12 | 5.64 | 0.84 |
| P1C | 1.54 | 12.33 | 0.44 | 79.39 | 0.68 | 90.59 | 148.72 | 26.67 | 16.05 | 13.44 | 0.85 |
| P1E | 2.22 | 10.14 | 0.37 | 80.22 | 0.55 | 89.80 | 160.12 | 15.13 | 9.93 | 8.49 | 0.88 |
| P1G | 1.23 | 9.44 | 0.35 | 79.41 | 0.65 | 90.32 | 145.53 | 19.08 | 13.88 | 12.47 | 0.90 |
| P1H | 2.42 | 41.94 | 0.82 | 80.24 | 0.80 | 89.47 | 165.82 | 97.95 | 57.82 | 49.61 | 0.83 |
| P2C | 2.08 | 6.55 | 0.27 | 79.74 | 0.61 | 90.71 | 168.30 | 22.15 | 18.23 | 20.15 | 0.86 |
| P1N | 1.55 | 9.82 | 0.41 | 79.48 | 0.62 | 90.35 | 163.29 | 32.36 | 20.68 | 16.02 | 0.91 |
| P1P | 2.45 | 6.11 | 0.32 | 79.55 | 0.62 | 91.12 | 139.68 | 30.05 | 21.36 | 18.57 | 0.90 |
| P2U | 2.33 | 6.82 | 0.30 | 79.37 | 0.63 | 90.98 | 188.66 | 26.46 | 19.59 | 19.50 | 0.86 |
| P2A | 1.32 | 10.64 | 0.39 | 79.60 | 0.67 | 90.55 | 157.50 | 27.95 | 18.64 | 17.92 | 0.83 |
| P2S | 2.15 | 10.55 | 0.31 | 79.80 | 0.62 | 90.64 | 165.70 | 30.72 | 22.59 | 20.85 | 0.89 |
| P3A | 1.68 | 7.22 | 0.24 | 80.04 | 0.59 | 89.48 | 120.74 | 22.97 | 14.69 | 15.21 | 0.79 |
| P3B | 1.64 | 7.13 | 0.31 | 80.28 | 0.52 | 88.98 | 109.76 | 20.46 | 14.29 | 12.70 | 0.89 |
| P3C | 1.77 | 8.00 | 0.28 | 80.13 | 0.62 | 89.76 | 131.59 | 43.54 | 31.70 | 27.30 | 0.92 |
| P3D | 1.94 | 5.60 | 0.28 | 80.10 | 0.61 | 89.57 | 130.01 | 24.15 | 16.46 | 14.36 | 0.88 |
| P3E | 2.23 | 8.20 | 0.34 | 79.86 | 0.62 | 89.75 | 131.11 | 34.05 | 23.81 | 22.59 | 0.86 |
| P3F | 2.22 | 8.00 | 0.42 | 80.00 | 0.63 | 89.58 | 118.04 | 46.10 | 29.80 | 28.61 | 0.82 |

**Table 4**
Geochemical characteristics of sediment derived from different provenance types (after McLennan et al., 1993; Girty et al., 1996),

| Provenance type | Eu/Eu* | Th/Sc | Th/U | Others |
|---|---|---|---|---|
| Old Upper continental crust | 0.6–1.1 | ≈1.0 | >3.8 | Evolved major compositions e.g. high Si/Al, CIA, high LILE uniform composition |
| Recycled sedimentary rocks | 0.6–1.1 | ≥1.0 | >3.8 | Evidence of heavy mineral concentration from trace elements e.g. Zr, Hf for Zircon |
| Young Differentiated Arc | 0.5–0.9 | ≈1.0 to 0.01 | <3.0 | Evolved major element compositions e.g. High Si/Al, CIA, high LILE abundance variable compositions |
| Young Undifferentiated Arc | ≈1.0 | ≈1.0 to 0.01 | <3.0 | Unevolved major element compositions e.g. low Si/Al, CIA, low LILE |

Furthermore, the compositional attributes of the sandstones, including monocrystalline quartz grains and the prevalence of non-undulatory quartz, suggest that the sediments were likely sourced from granitic and/or gneissic rocks (Tortosa et al., 1991).

Chemical weathering significantly influences the compositional attributes of siliciclastic sedimentary rocks. During weathering, cations such as Sr, Ca, and Na are preferentially leached from feldspars, whereas larger cations like Rb and Ba remain concentrated in the weathered residue (Elzien et al., 2014; Nesbitt et al., 1980). The preserved geochemical signatures in sedimentary rocks provide critical insights into the intensity and nature of chemical weathering processes in the source region (Fedo et al., 1996). The extent of weathering is often assessed by analyzing the relationship between alkaline earth metals and alkali metals (Nesbitt and Young, 1982). The $SiO_2/Al_2O_3$ versus $K_2O/Na_2O$ bivariate diagram serves as a robust tool for evaluating the compositional characteristics of sedimentary rocks (Maynard and Yu, 1982). This geochemical approach offers valuable information regarding the provenance and depositional environments of siliciclastic sedimentary units. This geochemical plot can provide insightful information about the provenance sources and depositional environments associated with these siliciclastic sedimentary units.

In the $SiO_2/Al_2O_3$ versus $K_2O/Na_2O$ diagram (Fig. 8b), the Noyem-

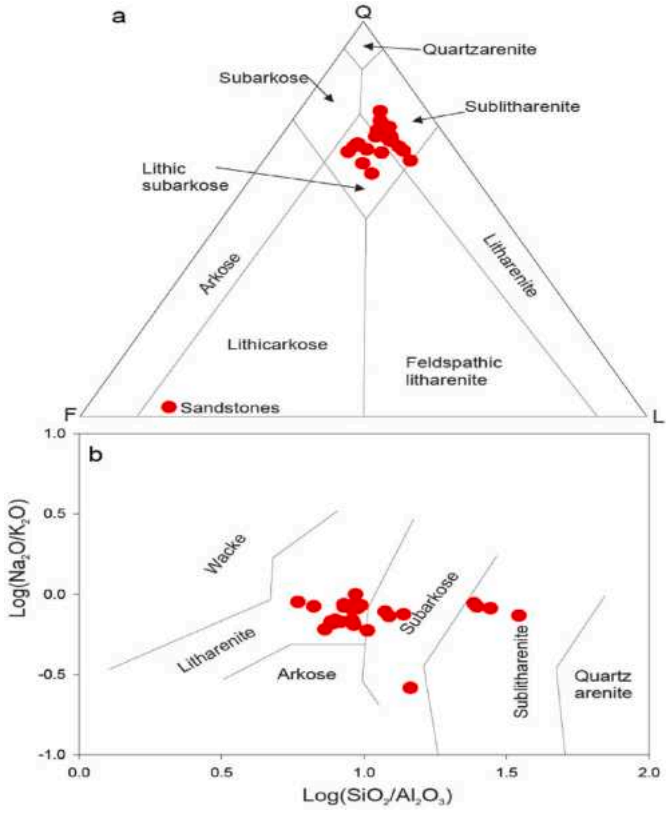


**Fig. 8.** (a) Q-F-L plot showing the effects of the composition of the source rock on the Noyem sandstones (fields after Pettijohn et al., 1987). **(b)** Binary chemical classification of Noyem sandstone samples: Log ($SiO_2/Al_2O_3$) vs Log ($Fe_2O_3/K_2O$) (fields after, Herron (1988).

Nyafoman sandstones are plotted within the litharenite, sub-arkose, and sub-lithic arenite fields, suggesting a composition enriched in lithic fragments with relatively lower proportions of feldspar and matrix. This compositional trend indicates a provenance linked to a

proximal orogenic source with a notable input of recycled or reworked material (Herron, 1988).

Additionally, this pattern aligns with a mature sedimentary system, characterized by moderate levels of weathering and erosion reflected in the sedimentary record (Pettijohn et al., 1987).

The calculated Chemical Index of Alteration (CIA) values for the Noyem-Nyafoman sandstones range from 77 to 80, with an average of 80 (Appendix). These elevated CIA values signify a moderate to high degree of chemical weathering and alteration (Nesbitt and Young, 1982). The degree of weathering is further elucidated using the $Al_2O_3$ – (CaO* + $Na_2O$)–$K_2O$ (A–CN–K) ternary diagram (Fig. 9a), where the sandstones plot along the pre-metasomatized trend and near the A–K join. Geochemical weathering trends in sedimentary rocks commonly align parallel to the A–CN join, reflecting the preferential depletion of mobile elements such as Ca and Na relative to immobile elements like Al during progressive weathering (Nesbitt and Young, 1982).

The Plagioclase Index of Alteration (PIA) and the Chemical Index of Weathering (CIW) are valuable geochemical proxies for evaluating the effects of potassium remobilization in weathered residues (Harnois, 1988; Fedo et al., 1995). For the Noyem-Nyafoman sandstones, the average PIA and CIW values range from 88 to 91 and 89 to 93, respectively (Appendix), suggesting moderate weathering in their source region (Fedo et al., 1995). Additionally, McLennan et al. (1993) proposed the Th/U versus Th plot as a means to assess the impact of weathering on the geochemical composition of siliciclastic sedimentary rocks. Their study demonstrated that intense chemical weathering elevates Th/U ratios as a result of the oxidation of $U^{4+}$ to $U^{6+}$ which promotes uranium loss from sediments. This process leads to Th/U values exceeding those typically observed in upper crustal igneous rocks, which generally range between 3.5 and 4.0 (McLennan et al., 1993).

A comparison of these findings with the current study reveals that the Noyem sandstones display moderate Th/U values ranging from 0.91 to 3.62 (average = 1.79), which are lower than those typically observed in upper crustal igneous rocks. This suggests a moderate degree of chemical weathering (Appendix). On the Th/U versus Th diagram (Fig. 9b) based on McLennan et al. (1993), the studied sandstones plot along a trajectory indicative of a depleted mantle source (Table 4). Additionally, the Compositional Variability Index (ICV) was employed to evaluate the relationship between major cation content and alumina in the sediments. This approach considers quartz dilution and provides insights into the extent of weathering processes at the source region (Cox et al., 1995).

The Index of Compositional Variability (ICV) is calculated using the formula: ICV = [CaO + $K_2O$ + $Na_2O$ + $Fe_2O_3$ (t) + MgO + MnO + $TiO_2$]/$Al_2O_3$, expressed as a weight percentage (%), where $Fe_2O_3$ (t) represents total iron and CaO denotes calcium. According to Li et al. (2013), lower ICV values indicate intensified weathering at the sediment source. Typical ICV values for granite and basalt average 0.95 and 2.2,

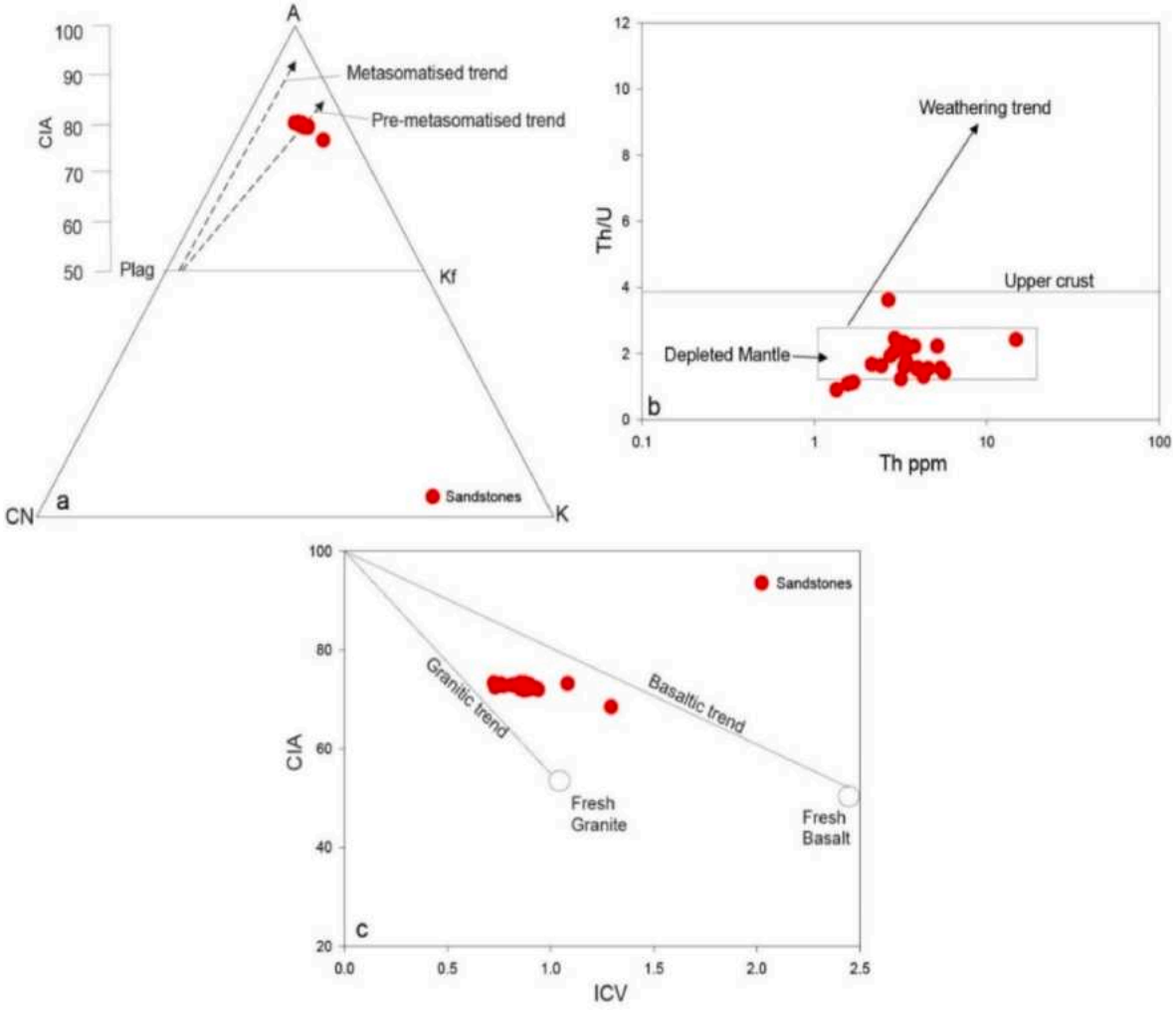


**Fig. 9.** (a) A-CN-K Ternary plot showing the weathering conditions of the studied sandstones (after Nesbitt and Young, 1984, 1989). (b) Binary plot of Th against Th/U indicating the source area weathering of the Noyem sandstone samples (after McLennan et al., 1993). (c) CIA versus ICV Plot for studied sandstones of Tarkwaian Group from the Northeastern extent of the Ashanti Belt, Ghana (after Potter et al., 2005).

respectively (Li et al., 2013). In this study, the sandstones exhibit low ICV values ranging from 0.52 to 0.94, with an average of 0.63 (Table 3), suggesting substantial chemical weathering at the source (Weaver et al., 1989). Furthermore, a binary plot of Chemical Index of Alteration (CIA) versus ICV values, as adapted from Sakyi et al. (2019) (Fig. 9c), shows that most of the sandstones closely follow the compositional trend for granite. This alignment implies a granitic source rock composition inferred from the ICV values. Consequently, the studied sandstones are likely derived from the adjacent Birimian Supergroup, which predominantly consists of granitoids within the study area.

The La/Th versus Hf diagram is a valuable tool in provenance studies for determining the composition of parent rocks (Floyd and Leveridge, 1987). In this study, the analyzed samples predominantly plot within the andesitic and mixed felsic/mafic source fields (Fig. 10a), suggesting that the parent rocks are primarily of intermediate to felsic composition. Andesite, an intermediate volcanic rock, is typically associated with subduction-related magmatism in continental arc or island arc tectonic settings (Rollinson, 1993). This indicates that the parent rocks of these samples were likely derived from a magmatic arc environment (Floyd and Leveridge, 1987). However, a few samples plot within the mafic source field, implying a minor contribution from mafic rocks.

Additionally, the Co/Th versus La/Sc diagram, as proposed by McLennan and Taylor (1991), is extensively used in provenance research to infer source rock compositions. In the present study, this diagram (Fig. 10b) shows that all the Noyem sandstones plot between the andesite and felsic volcanic rock fields. This further confirms that the source rocks are predominantly of intermediate to felsic composition, consistent with the inferred lithology of the source area.

### 5.3. Tectonic setting

The tectonic setting of sediments can be effectively determined by integrating petrographic studies, heavy mineral analysis, geochemical data, and detrital geochronology. This multidisciplinary approach enables the reconstruction of sediment provenance, tectonic history, and paleogeographic evolution (Garzanti, 2019). A thorough understanding of sedimentary processes is essential to accurately interpret tectonic settings and associated basin evolution, particularly in identifying recycled orogenic sediments (Garzanti, 2019).

Previous studies have established correlations between detrital sandstone compositions and major provenance categories, including magmatic arcs, recycled orogens, basement uplifts, and stable cratons (Dickinson and Suczek, 1979; Dickinson et al., 1983). According to Dickinson et al. (1983), the Q-F-L ternary diagram provides insights into the characteristics of parent rocks. In the current study, the investigated samples predominantly plot within the recycled orogen field on the Q-F-L ternary diagram (Fig. 11a). This suggests that the sediments were derived from moderately mature to mature sources, indicative of deposition in a relatively stable to active continental margin tectonic setting (Dickinson, 1970).

Dickinson et al. (1983) noted that mature sandstones in this region are typically derived from underlying gneissic and granitoid sources. Several studies (Bhatia, 1983; Roser and Korsch, 1986; McLennan et al., 1990; Armstrong-Altrin et al., 2015) have employed the geochemical composition of sandstones to distinguish between different tectonic settings. Armstrong-Altrin et al. (2015) introduced two multidimensional discrimination diagrams for sandstones with high silica content ($SiO_2$ adjusted = 63–95%) and low silica content ($SiO_2$ adjusted = 35–63%) to differentiate among arc (island and continental), rift, and collisional tectonic settings.

In the high-silica ($SiO_2$ adjusted = 63–95%) diagram, the studied sandstones plot within the Arc field (Fig. 11b), suggesting that the sediments were sourced from an active continental margin or magmatic arc setting (Dickinson and Suczek, 1979; Dickinson, 1970). This implies that the provenance of the sandstones was influenced by active tectonic processes such as subduction, mountain building, and associated plutonic and volcanic activities. Additionally, the Ti/Zr versus La/Sc tectonic discrimination diagram provides another robust method for evaluating the tectonic settings of siliciclastic sedimentary rocks (Bhatia, 1983; Bhatia and Crook, 1986).

The positioning of the studied sandstoness on the Ti/Zr versus La/Sc diagram (Fig. 11c) reveals that the majority of samples plot within or near the continental arc and active continental margin domains, with a few samples falling within the passive margin domain. Similarly, on the Th-Sc-Zr/10 tectonic discrimination diagram, most sandstones from the Noyem-Nyafoman Gold Project area plot within or near the continental island arc domain (Fig. 11d) (Bhatia, 1983; Condie, 1989). These findings suggest that the primary tectonic setting of sediment deposition was an active margin, such as a continental arc environment, with minor contributions from a passive margin-related setting (Bhatia, 1983). The compositional characteristics of the analyzed sandstones, particularly the abundance of quartz grains, including monocrystalline quartz and a dominance of non-undulatory quartz, further indicate that these sediments were likely derived from granitic and/or gneissic source rocks (Tortosa et al., 1991).

The predominance of non-undulose monocrystalline quartz grains in the studied sandstones suggests derivation primarily from plutonic rocks (Basu et al., 1975). This inference is further supported by the presence of quartz grains containing inclusions of heavy minerals, which points to granitic sources (Morton and Hallsworth, 1994). Geochemical analysis of sediments provides critical insights into source rock compositions, with major oxides serving as indicators of parent rock characteristics

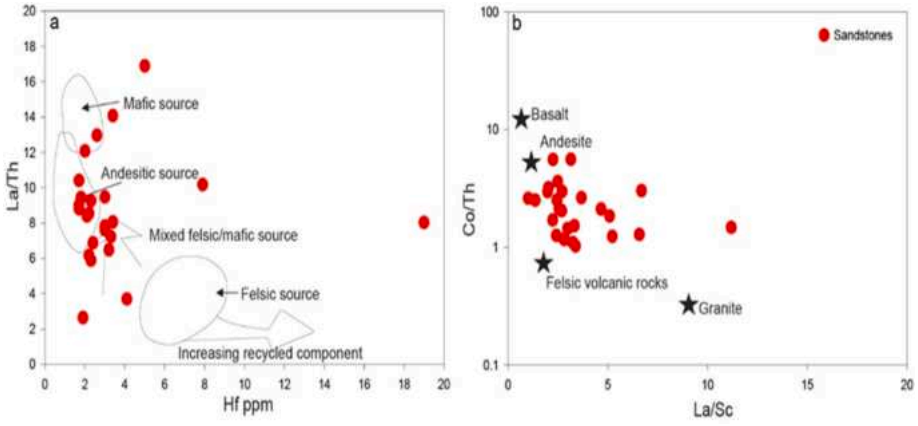


**Fig. 10.** (a) The La/Th-Hf Diagram for the studied sandstones (after Floyd and Leveridge (1987), (b) The Co/Th vs La/Sc Diagram (after McLennan and Taylor (1991).

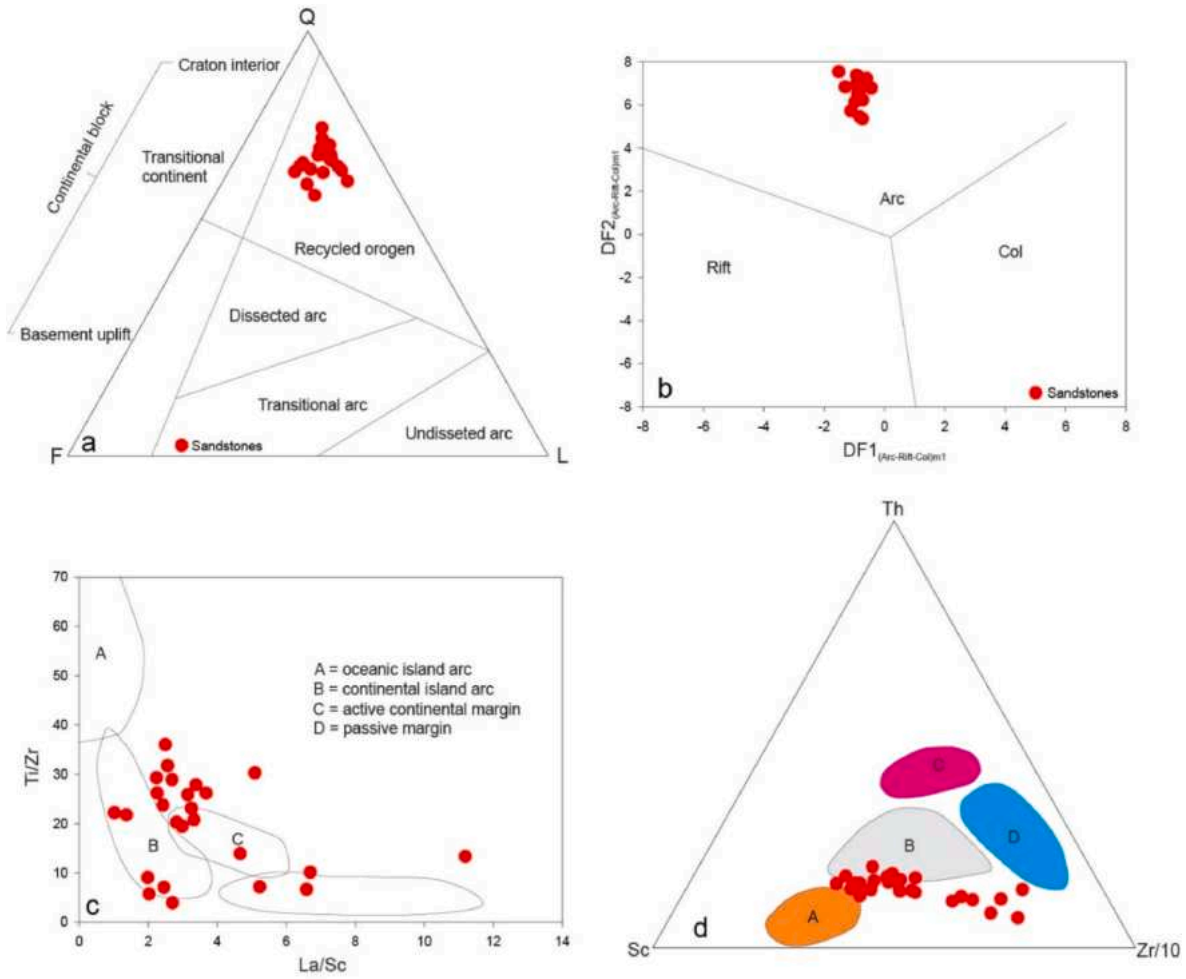


**Fig. 11.** (a) QFL plots for sandstones from the studied sandstones (after Dickinson et al., 1983). (b) DF1 versus DF2 discriminant function diagram (after Dickinson et al. (1983). (c) Ti/Zr versus La/Sc Tectonic Discrimination plot (after Bhatia, 1983). (d) The Th-Sc-Zr/10 geochemical plot (after, Bhatia, 1983; Bhatia and Crook, 1986).

(Weltje and von Eynatten, 2004). For instance, the $Al_2O_3/TiO_2$ ratio is a reliable parameter for determining source rock composition (Hayashi et al., 1997; Nagarajan et al., 2007). In this study, the Noyem sandstones exhibit high $Al_2O_3/TiO_2$ ratios ranging from 15.55 to 33.50, with an average of 26.61 (Table 3), indicative of felsic rock provenance (Hayashi et al., 1997).

Moreover, the elevated $SiO_2$ content in the sandstones, ranging from 74.70 to 94.70 wt% (average = 84.88 wt%), suggests that the sediments were derived from granitic sources or acidic high-grade metamorphic rocks (Basu et al., 1975). The relatively lower primitive chondrite-normalized values (Fig. 12a) indicate that the source rocks underwent significant enrichment through weathering and/or sedimentary recycling. This observation aligns with the negative correlations between $SiO_2$ and $Al_2O_3$, MgO, and $K_2O$ (Fig. 6).

When normalized against average Upper Continental Crust (UCC) values, most trace elements in the Noyem sandstones show enrichment relative to the UCC across the analyzed samples (Fig. 12b), further highlighting the geochemical maturity and evolved nature of the source rocks.

The enrichment of light rare earth elements (LREE) relative to middle rare earth elements (MREE) and heavy rare earth elements (HREE) suggests that the sediments forming the sandstones were primarily derived from continental rather than oceanic sources (Abu and Sunkari, 2020b). Across all analyzed samples, a consistent LREE enrichment is observed relative to MREE, coupled with relatively flat to slightly depleted HREE patterns and predominantly negative Eu anomalies.

Chondrite-normalized rare earth element (REE) patterns of the Noyem sandstones show similarities to those of Post-Archean Australian Shale (PAAS) and the Upper Continental Crust (UCC). However, most samples display REE depletion compared to PAAS and UCC, likely attributed to quartz dilution. These findings provide valuable insights into the trace element composition and rare earth element distribution in the Noyem sandstones, offering a deeper understanding of their provenance and depositional history.

### 5.4. *Implication for the crustal evolution*

The chemical composition of rocks undergoes significant trace element variations between the Archean and post-Archean upper crust as a result of crustal evolution. These changes are reflected in the geochemical characteristics of the sediments (Condie et al., 1992). Key geochemical attributes observed include.

- Decrease in Eu anomalies
- Reduction in GdN/YbN values from >2 to 1.0–2.0
- Decrease in Sm/Nd ratio within the range of about 0.21 to 0.19
- Decrease in Cr/Th values from about 20.0 to 5.7
- Decrease in Cr/Sc values from about 13 to 4.1
- Increase in Th/Sc values from about 0.5 to 1.0

These variations are attributed to sedimentary processes affecting the source rocks or sediments (Plank and Langmuir, 1998; Asiedu et al.,

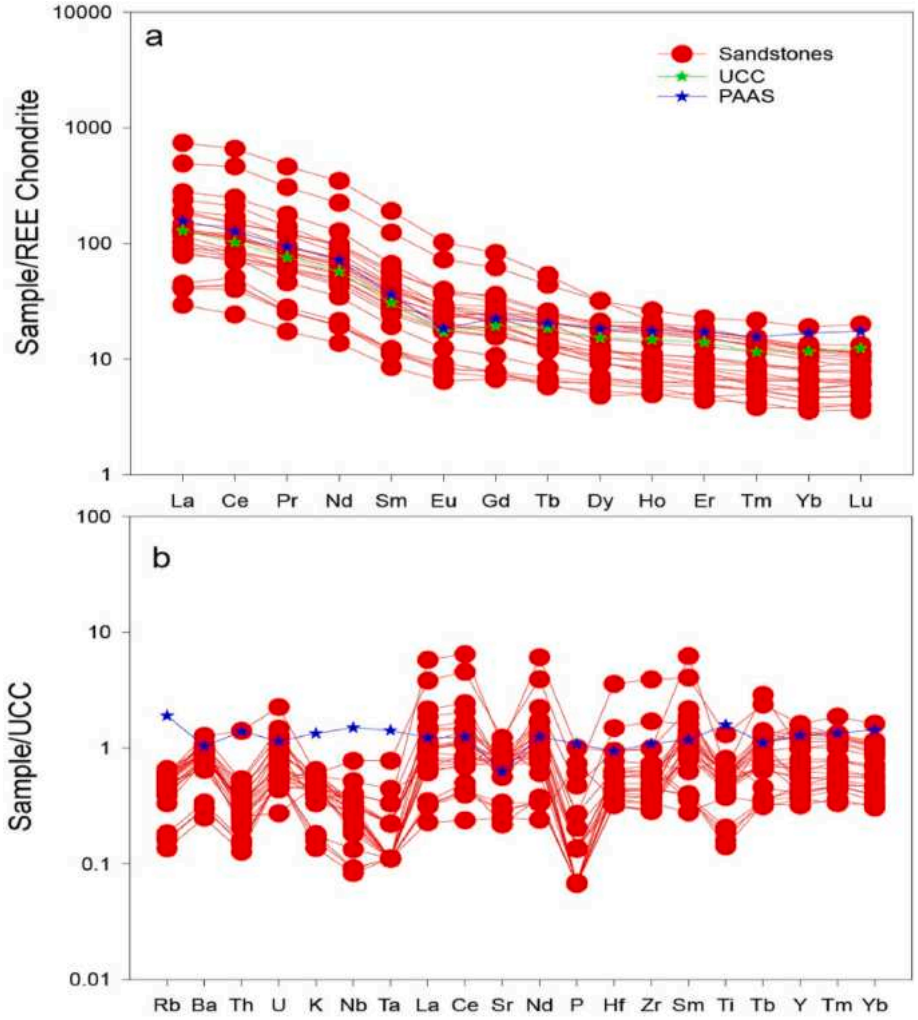


**Fig. 12(a).** Chondrite normalized REE plot of the Noyem sandstones (Normalization values after Boynton, 1984) (b) UCC-normalized plot for the Noyem sandstones (Normalization values after Taylor et al., 1992).

2019). The dilution of marine terrigenous sediments with siliceous and carbonate sediments, which are low in trace element content, may explain the changes observed in the chemical composition of the upper crust (Plank and Langmuir, 1998). Studies on the Birimian metasediments, part of the Precambrian shields, conducted by Abouchami et al. (1990), Leube et al. (1990), Sylvester and Attoh (1992), Taylor et al. (1992), and Asiedu et al. (2004), indicate that the continental crust of Ghana (and possibly West Africa) during the early Proterozoic era exhibited a composition closely resembling that of the Archean crust. In comparison, the Noyem-Nyafoman sandstones from the Tarkwaian Group at the northeastern extent of the Ashanti Belt exhibit trace element variations that are characteristic of post-Archean sedimentary rocks.

The analyzed sandstones exhibit relatively low average Eu anomalies, with values ranging from 0.87 to 0.96 (average Eu/Eu* = 0.87), a slight decrease in GdN/YbN ratios ranging from 1.01 to 14.53 (average = 2.74), and a reduced Sm/Nd ratio ranging from 0.17 to 0.20 (average = 0.19). Additionally, there is a moderate increase in Cr/Sc ratios, ranging from 5.45 to 12.0 (average = 8.04), and a reduction in Th/Sc values, which range from 0.24 to 0.82 (average = 0.37) (Appendix). When compared to the findings of McLennan and Taylor (1991), these geochemical signatures suggest significant compositional variations over time.

The observed geochemical patterns provide critical insights into crustal evolution and provenance. The relatively low Eu anomalies, decreasing GdN/YbN and Sm/Nd ratios, moderate Cr/Sc increases, and declining Th/Sc values (Tables 4 and 5) collectively indicate a complex history of crustal development and source area characteristics. These variations likely reflect differences in the original composition of source rocks, tectonic settings, or weathering processes over geological time, offering valuable information on the geological evolution of the studied terrane (Condie et al., 1992; McLennan and Taylor, 1991).

**Table 5**
Range of elemental ratios of Noyem sandstones compared to the ratios in similar fractions derived from felsic rocks, mafic rocks, Upper Continental Crust, (UCC) and post–Archean Australian average shale (PAAS) (Cullers, 1988; Cullers, 1994, 2000; Cullers & Podkovyrov, 2000)

| Elemental ratios | Noyem sandstones | Range of sediments | | UCC | PAAS |
|---|---|---|---|---|---|
| | | Felsic rocks | Mafic rocks | | |
| Th/Sc | 0.24–0.82 | 0.84–20.5 | 0.05–0.22 | 0.79 | 0.90 |
| Th/Co | 0.18 -0.97 | 0.67–19.4 | 0.04–1.4 | 0.63 | 0.63 |
| Th/Cr | 0.03- 0.07 | 0.13–2.7 | 0.02–0.05 | 0.13 | 0.13 |
| Cr/Th | 15.15–35.71 | 4.0–15.0 | 25–500 | 7.76 | 7.53 |
| La/Sc | 1.01–11.19 | 2.5–16.3 | 0.43–0.86 | 2.21 | 2.40 |

## 6. Conclusion

The tectonic setting, provenance, source area weathering, and source rock composition of the Noyem sandstones within the Tarkwaian Group at the northeastern extent of the Ashanti Belt, Ghana, were comprehensively evaluated using integrated petrographic and geochemical analyses. Based on these assessments, the following conclusions have been derived.

- The major element compositions and petrographic characteristics of the samples from the northeastern extent of the Ashanti Belt classify the Noyem-Nyafoman sediments as litharenites, sublitharenites, and quartz arenites.
- The presence of polycrystalline quartz grains, significant sedimentary clasts, and fragments of sedimentary rocks (including sandstones, conglomerates, and breccias) indicates a heterogeneous origin, likely derived from both metamorphic and sedimentary sources, with potential contributions of trace elements from magmatic origins.
- The calculated Chemical Index of Alteration (CIA) values suggest moderate to high levels of chemical weathering and alteration at the source area.

The major element composition, combined with tectonic discrimination diagrams, suggests that the Noyem sandstones were deposited in an active tectonic setting, such as a continental arc environment.

- Geochemical analysis of trace element compositions and their relative proportions indicates that the Noyem-Nyafoman sandstones are predominantly intermediate to felsic in nature, with potential contributions from mafic sources. This interpretation is supported by comparisons of observed trace element ratios with established benchmarks for felsic and mafic rock types, such as the Post-Archean Australian Shales (PAAS) and the Upper Continental Crust (UCC), as reported in previous studies.
- Rare earth element (REE) patterns, along with Eu/Eu*, La/Sc, Th/Sc, Cr/Th, and Th/Sc ratios, further suggest that the Noyem sandstones were derived from a mixed source, encompassing both intermediate and felsic rocks.

## CRediT authorship contribution statement

**Victor Sedziafa:** Writing – review & editing, Writing – original draft, Visualization, Software, Project administration, Methodology, Investigation, Funding acquisition, Formal analysis, Data curation, Conceptualization. **Ying Song:** Writing – original draft, Validation, Supervision, Project administration, Methodology, Conceptualization. **Emmanuel Daanoba Sunkari:** Writing – review & editing, Writing – original draft, Investigation, Formal analysis, Data curation. **Daniel Kwayisi:** Writing – review & editing, Writing – original draft, Visualization, Software, Investigation, Data curation. **Chris Y. Anani:** Writing – original draft, Supervision. **Daniel K. Asiedu:** Writing – review & editing, Writing – original draft, Supervision, Conceptualization.

## Declaration of competing interest

The authors declare that they have no known competing financial interests or personal relationships that could have appeared to influence the work reported in this paper.

## Acknowledgment

The authors extend their gratitude to all individuals whose invaluable contributions, insightful edits, and constructive feedback significantly enhanced the quality of this research. Financial support for this study was jointly provided by the Department of Earth Science Capacity Building Fund at the University of Ghana, Legon-Accra, and the National Natural Science Foundation of China (42172114). This research forms part of the first author's MPhil thesis and is integrated into ongoing PhD research at the Geology Department, China University of Petroleum, East China.

## Appendix

Major elements, trace elements, rare earth elements, and normalization data for the analyzed samples.

| Samples | Chemical analysis of major elements (wt.%), trace elements (ppm), and rare earth elements (REEs) of the analyzed sandstones | | | | | | | | | | | | |
|---|---|---|---|---|---|---|---|---|---|---|---|---|---|
| | P1B | P1C | P1D | P1E | P1F | P1G | P1H | P1J | P2C | P1K | P1O | P1N | P1M |
| **Major oxides** | | | | | | | | | | | | | |
| $SiO_2$ | 85.70 | 83.40 | 93.00 | 78.60 | 94.70 | 82.90 | 74.70 | 87.80 | 82.30 | 87.20 | 92.80 | 81.60 | 88.10 |
| $Al_2O_3$ | 9.04 | 9.05 | 3.35 | 11.80 | 2.71 | 9.14 | 12.75 | 7.18 | 10.55 | 7.36 | 3.73 | 10.30 | 6.40 |
| $Fe_2O_3$ | 2.25 | 3.30 | 1.17 | 2.94 | 0.96 | 3.09 | 6.04 | 1.60 | 3.32 | 2.20 | 1.28 | 3.18 | 1.98 |
| CaO | 0.05 | 0.03 | 0.02 | 0.02 | 0.01 | 0.02 | 0.03 | 0.02 | 0.02 | 0.02 | 0.01 | 0.02 | 0.02 |
| MgO | 0.09 | 0.11 | 0.03 | 0.10 | 0.03 | 0.10 | 0.12 | 0.06 | 0.11 | 0.06 | 0.03 | 0.11 | 0.06 |
| $Na_2O$ | 1.00 | 0.91 | 0.36 | 1.32 | 0.28 | 0.96 | 1.47 | 0.76 | 1.06 | 0.81 | 0.42 | 1.08 | 0.69 |
| $K_2O$ | 1.22 | 1.41 | 0.44 | 1.57 | 0.38 | 1.39 | 1.64 | 1.04 | 1.6 | 1.04 | 0.5 | 1.56 | 0.92 |
| $Cr_2O_3$ | 0.01 | 0.01 | 0.01 | 0.02 | 0.01 | 0.01 | 0.04 | 0.01 | 0.01 | 0.01 | 0.01 | 0.01 | 0.01 |
| $TiO_2$ | 0.42 | 0.38 | 0.1 | 0.5 | 0.09 | 0.33 | 0.82 | 0.28 | 0.35 | 0.39 | 0.12 | 0.41 | 0.32 |
| MnO | 0.01 | 0.02 | 0.01 | 0.01 | 0.01 | 0.01 | 0.04 | 0.01 | 0.01 | 0.01 | 0.01 | 0.01 | 0.1 |
| $P_2O_5$ | 0.15 | 0.02 | 0.01 | 0.01 | 0.01 | 0.01 | 0.09 | 0.04 | 0.01 | 0.04 | 0.01 | 0.02 | 0.07 |
| SrO | 0.04 | 0.02 | 0.01 | 0.04 | 0.01 | 0.03 | 0.05 | 0.02 | 0.02 | 0.02 | 0.01 | 0.03 | 0.02 |
| BaO | 0.1 | 0.07 | 0.02 | 0.08 | 0.02 | 0.07 | 0.1 | 0.06 | 0.07 | 0.06 | 0.03 | 0.08 | 0.06 |
| LOI | 1.34 | 1.25 | 0.51 | 1.64 | 0.37 | 1.33 | 1.78 | 1.03 | 1.48 | 1.05 | 0.57 | 1.42 | 1.01 |
| **Total** | **101.42** | **99.98** | **99.02** | **98.64** | **99.58** | **99.38** | **99.67** | **99.91** | **100.9** | **100.26** | **99.52** | **99.82** | **99.76** |
| CIA | 75.50 | 74.78 | 75.46 | 75.20 | 75.51 | 74.64 | 75.34 | 75.13 | 75.11 | 74.96 | 75.06 | 74.75 | 75.19 |
| PIA | 88.16 | 89.04 | 88.45 | 88.42 | 88.93 | 88.77 | 88.10 | 88.73 | 89.23 | 88.39 | 88.25 | 88.82 | 88.53 |
| CIW | 89.59 | 90.59 | 89.81 | 89.80 | 90.33 | 90.32 | 89.47 | 90.20 | 90.71 | 89.87 | 89.66 | 90.35 | 90.01 |
| ICV | 0.56 | 0.68 | 0.64 | 0.55 | 0.65 | 0.65 | 0.80 | 0.53 | 0.61 | 0.62 | 0.64 | 0.62 | 0.64 |
| $SiO_2/Al_2O_3$ | 9.48 | 9.22 | 27.76 | 6.66 | 34.94 | 9.07 | 5.86 | 12.23 | 7.80 | 11.85 | 24.88 | 7.92 | 13.77 |
| $K_2O/Na_2O$ | 1.22 | 1.55 | 1.22 | 1.19 | 1.36 | 1.45 | 1.12 | 1.37 | 1.51 | 1.28 | 1.19 | 1.44 | 1.33 |

(*continued on next page*)

(*continued*)

| Samples | Chemical analysis of major elements (wt.%), trace elements (ppm), and rare earth elements (REEs) of the analyzed sandstones | | | | | | | | | | | | |
|---|---|---|---|---|---|---|---|---|---|---|---|---|---|
| | P1B | P1C | P1D | P1E | P1F | P1G | P1H | P1J | P2C | P1K | P1O | P1N | P1M |
| $K_2O/Al_2O_3$ | 0.13 | 0.16 | 0.13 | 0.13 | 0.14 | 0.15 | 0.13 | 0.14 | 0.15 | 0.14 | 0.13 | 0.15 | 0.14 |
| $Al_2O_3/TiO_2$ | 21.52 | 23.82 | 33.50 | 23.60 | 30.11 | 27.70 | 15.55 | 25.64 | 30.14 | 18.87 | 31.08 | 25.12 | 20.00 |
| **Trace elements** | | | | | | | | | | | | | |
| V | 50.00 | 61.00 | 19.00 | 73.00 | 15.00 | 57.00 | 94.00 | 42.00 | 59.00 | 48.00 | 17.00 | 66.00 | 38.00 |
| Cr | 100.00 | 90.00 | 30.00 | 160.00 | 30.00 | 90.00 | 310.00 | 60.00 | 60.00 | 100.00 | 40.00 | 80.00 | 60.00 |
| Co | 8.00 | 6.00 | 4.00 | 13.00 | 4.00 | 4.00 | 19.00 | 7.00 | 5.00 | 7.00 | 5.00 | 5.00 | 12.00 |
| Ni | 22.00 | 10.00 | 6.00 | 24.00 | 6.00 | 11.00 | 39.00 | 15.00 | 7.00 | 16.00 | 8.00 | 11.00 | 31.00 |
| Cu | 4.00 | 3.00 | 1.00 | 2.00 | 1.00 | 1.00 | 30.00 | 4.00 | 3.00 | 2.00 | 1.00 | 1.00 | 17.00 |
| Rb | 38.00 | 45.70 | 13.90 | 50.00 | 11.40 | 43.90 | 50.50 | 32.90 | 49.30 | 33.00 | 13.50 | 50.70 | 28.00 |
| Sr | 338.00 | 222.00 | 93.70 | 336.00 | 70.00 | 227.0 | 392.0 | 220.0 | 224.00 | 222.00 | 92.80 | 263.0 | 218.0 |
| Cs | 1.44 | 1.83 | 0.54 | 1.91 | 0.42 | 1.76 | 1.95 | 1.26 | 1.88 | 1.19 | 0.50 | 2.01 | 1.05 |
| Ba | 799.00 | 608.00 | 190.00 | 651.00 | 157.00 | 575.00 | 95.00 | 52.00 | 557.00 | 501.00 | 189.00 | 675.00 | 488.00 |
| Y | 20.60 | 11.60 | 8.90 | 8.50 | 6.70 | 15.90 | 33.90 | 8.90 | 33.40 | 13.00 | 7.60 | 13.30 | 10.10 |
| Zr | 189.00 | 111.00 | 86.00 | 142.00 | 138.00 | 85.00 | 755.00 | 122.00 | 72.00 | 329.00 | 127.00 | 108.0 | 192.0 |
| Hf | 5.00 | 3.00 | 2.20 | 4.10 | 3.40 | 2.40 | 19.00 | 3.40 | 2.10 | 7.90 | 3.20 | 3.00 | 5.00 |
| Nb | 4.90 | 3.90 | 1.10 | 6.20 | 1.00 | 3.30 | 9.30 | 3.20 | 3.40 | 4.80 | 1.10 | 4.30 | 3.50 |
| Ta | 0.30 | 0.20 | <0.1 | 0.40 | <0.1 | 0.10 | 0.70 | 0.10 | 0.10 | 0.30 | <0.1 | 0.20 | 0.10 |
| Sc | 16.00 | 9.00 | 4.00 | 14.00 | 4.00 | 9.00 | 18.00 | 10.00 | 11.00 | 11.00 | 5.00 | 11.00 | 10.00 |
| Th | 5.41 | 3.93 | 1.59 | 5.16 | 1.34 | 3.17 | 14.75 | 3.31 | 2.93 | 5.65 | 1.56 | 4.56 | 3.96 |
| **REEs** | | | | | | | | | | | | | |
| La | 179.00 | 29.90 | 9.80 | 19.10 | 10.80 | 21.80 | 118.50 | 46.60 | 24.60 | 57.50 | 10.10 | 35.70 | 66.90 |
| Ce | 408.00 | 69.10 | 24.90 | 45.90 | 31.50 | 53.10 | 287.00 | 106.50 | 46.80 | 130.50 | 27.30 | 86.00 | 154.00 |
| Pr | 43.40 | 7.42 | 2.40 | 4.31 | 2.61 | 5.45 | 28.80 | 11.10 | 5.88 | 13.15 | 2.40 | 8.92 | 16.65 |
| Nd | 164.50 | 28.60 | 9.30 | 16.40 | 10.10 | 20.40 | 106.00 | 38.80 | 23.10 | 44.40 | 9.20 | 35.10 | 60.20 |
| Sm | 29.30 | 5.20 | 1.88 | 2.95 | 1.84 | 3.72 | 19.10 | 6.76 | 4.32 | 7.55 | 1.69 | 6.31 | 10.20 |
| Eu | 6.02 | 1.18 | 0.48 | 0.73 | 0.54 | 1.02 | 4.25 | 1.49 | 1.34 | 1.67 | 0.49 | 1.52 | 2.22 |
| Gd | 17.15 | 3.48 | 1.63 | 2.20 | 1.61 | 3.23 | 12.85 | 4.33 | 5.22 | 4.85 | 1.60 | 4.15 | 6.41 |
| Tb | 2.02 | 0.45 | 0.26 | 0.32 | 0.23 | 0.49 | 1.66 | 0.52 | 0.89 | 0.61 | 0.22 | 0.52 | 0.79 |
| Dy | 8.16 | 2.34 | 1.67 | 1.81 | 1.23 | 3.01 | 8.18 | 2.45 | 5.38 | 3.12 | 1.35 | 2.68 | 3.27 |
| Ho | 1.20 | 0.46 | 0.37 | 0.33 | 0.28 | 0.62 | 1.49 | 0.42 | 1.16 | 0.58 | 0.28 | 0.52 | 0.51 |
| Er | 2.58 | 1.21 | 0.98 | 0.97 | 0.73 | 1.69 | 3.73 | 1.01 | 3.06 | 1.52 | 0.83 | 1.35 | 1.30 |
| Tm | 0.33 | 0.17 | 0.14 | 0.14 | 0.11 | 0.23 | 0.56 | 0.14 | 0.39 | 0.23 | 0.10 | 0.18 | 0.15 |
| Yb | 1.77 | 1.09 | 0.79 | 0.94 | 0.60 | 1.32 | 3.18 | 0.77 | 2.25 | 1.41 | 0.64 | 1.15 | 0.89 |
| Lu | 0.24 | 0.15 | 0.12 | 0.15 | 0.09 | 0.19 | 0.50 | 0.12 | 0.33 | 0.24 | 0.10 | 0.16 | 0.13 |
| La/Sc | 11.19 | 3.32 | 2.45 | 1.36 | 2.70 | 2.42 | 6.58 | 4.66 | 2.24 | 5.23 | 2.02 | 3.25 | 6.69 |
| Th/Co | 0.68 | 0.66 | 0.40 | 0.40 | 0.34 | 0.79 | 0.78 | 0.47 | 0.59 | 0.81 | 0.31 | 0.91 | 0.33 |
| Rb/Sr | 0.11 | 0.21 | 0.15 | 0.15 | 0.16 | 0.19 | 0.13 | 0.15 | 0.22 | 0.15 | 0.15 | 0.19 | 0.13 |
| Th/U | 1.55 | 1.54 | 1.10 | 2.22 | 0.91 | 1.23 | 2.42 | 1.60 | 2.08 | 1.42 | 1.08 | 1.55 | 1.57 |
| Th/Sc | 0.34 | 0.44 | 0.40 | 0.37 | 0.34 | 0.35 | 0.82 | 0.33 | 0.27 | 0.51 | 0.31 | 0.41 | 0.40 |
| Cr/Th | 18.48 | 22.90 | 18.87 | 31.01 | 22.39 | 28.39 | 21.02 | 18.13 | 20.48 | 17.70 | 25.64 | 17.54 | 15.15 |
| Zr/Sc | 11.81 | 12.33 | 21.50 | 10.14 | 34.50 | 9.44 | 41.94 | 12.20 | 6.55 | 29.91 | 25.40 | 9.82 | 19.20 |
| Th/Cr | 0.05 | 0.04 | 0.05 | 0.03 | 0.04 | 0.04 | 0.05 | 0.06 | 0.05 | 0.06 | 0.04 | 0.06 | 0.07 |
| Sm/Nd | 0.18 | 0.18 | 0.20 | 0.18 | 0.18 | 0.18 | 0.18 | 0.17 | 0.19 | 0.17 | 0.18 | 0.18 | 0.17 |
| Cr/Sc | 6.25 | 10.00 | 7.50 | 11.43 | 7.50 | 10.00 | 17.22 | 6.00 | 5.45 | 9.09 | 8.00 | 7.27 | 6.00 |
| **∑REE** | 492.27 | 102.25 | 42.72 | 72.85 | 41.47 | 88.07 | 360.70 | 133.41 | 122.32 | 160.83 | 41.60 | 122.56 | 189.72 |
| LaN/YbN | 26.16 | 7.10 | 3.21 | 5.26 | 4.66 | 4.27 | 9.64 | 15.65 | 2.83 | 10.55 | 4.08 | 8.03 | 19.44 |
| LaN/SmN | 1.47 | 1.39 | 1.26 | 1.56 | 1.42 | 1.41 | 1.50 | 1.66 | 1.37 | 1.84 | 1.44 | 1.37 | 1.58 |
| GdN/YbN | 7.82 | 2.58 | 1.66 | 1.89 | 2.17 | 1.97 | 3.26 | 4.54 | 1.87 | 2.78 | 2.02 | 2.91 | 5.81 |
| Eu/Eu* | 0.82 | 0.85 | 0.84 | 0.88 | 0.96 | 0.90 | 0.83 | 0.84 | 0.86 | 0.84 | 0.91 | 0.91 | 0.84 |

| Samples | P1P | P1R | P2U | P2A | P2S | P3A | P3B | P3C | P3D | P3E | P3F | P3K |
|---|---|---|---|---|---|---|---|---|---|---|---|---|
| **Major oxides (wt.%)** | | | | | | | | | | | | |
| $SiO_2$ | 84.40 | 92.70 | 80.20 | 81.90 | 80.90 | 84.10 | 84.40 | 82.00 | 82.40 | 83.80 | 84.70 | 87.80 |
| $Al_2O_3$ | 8.21 | 3.81 | 11.00 | 9.87 | 10.55 | 9.02 | 9.04 | 9.64 | 9.70 | 9.28 | 8.68 | 6.04 |
| $Fe_2O_3$ | 2.58 | 1.26 | 3.53 | 3.60 | 3.39 | 2.64 | 2.14 | 3.03 | 2.99 | 2.88 | 2.85 | 3.43 |
| CaO | 0.02 | 0.01 | 0.02 | 0.02 | 0.02 | 0.02 | 0.02 | 0.02 | 0.02 | 0.02 | 0.02 | 0.14 |
| MgO | 0.10 | 0.03 | 0.12 | 0.11 | 0.11 | 0.08 | 0.08 | 0.10 | 0.10 | 0.09 | 0.08 | 0.15 |
| $Na_2O$ | 0.78 | 0.43 | 1.07 | 1.01 | 1.07 | 1.04 | 1.10 | 1.08 | 1.11 | 1.04 | 0.99 | 0.35 |
| $K_2O$ | 1.31 | 0.49 | 1.77 | 1.50 | 1.58 | 1.19 | 1.10 | 1.29 | 1.28 | 1.28 | 1.16 | 1.34 |
| $Cr_2O_3$ | 0.01 | 0.01 | 0.01 | 0.01 | 0.01 | 0.01 | 0.01 | 0.01 | 0.01 | 0.01 | 0.01 | 0.01 |
| $TiO_2$ | 0.25 | 0.13 | 0.39 | 0.39 | 0.37 | 0.28 | 0.27 | 0.41 | 0.33 | 0.35 | 0.36 | 0.24 |
| MnO | 0.01 | 0.01 | 0.01 | 0.01 | 0.01 | 0.06 | 0.01 | 0.09 | 0.04 | 0.10 | 0.05 | 0.01 |
| $P_2O_5$ | 0.01 | 0.01 | 0.01 | 0.01 | 0.02 | 0.02 | 0.01 | 0.03 | 0.01 | 0.02 | 0.02 | 0.11 |
| SrO | 0.02 | 0.01 | 0.02 | 0.03 | 0.03 | 0.03 | 0.03 | 0.03 | 0.03 | 0.03 | 0.03 | 0.01 |
| BaO | 0.07 | 0.02 | 0.08 | 0.08 | 0.07 | 0.06 | 0.05 | 0.07 | 0.06 | 0.07 | 0.06 | 0.05 |
| LOI | 1.23 | 0.59 | 1.60 | 1.36 | 1.49 | 1.28 | 1.35 | 1.41 | 1.37 | 1.33 | 1.29 | 0.90 |
| **Total** | **98.99** | **99.50** | **99.82** | **99.90** | **99.61** | **99.83** | **99.61** | **99.21** | **99.45** | **100.30** | **100.30** | **100.58** |
| CIA | 75.09 | 75.37 | 74.84 | 74.91 | 75.17 | 74.96 | 74.95 | 75.19 | 75.00 | 74.89 | 74.97 | 73.77 |
| PIA | 89.61 | 88.30 | 89.44 | 89.04 | 89.17 | 88.08 | 87.64 | 88.36 | 88.17 | 88.30 | 88.16 | 90.56 |
| CIW | 91.12 | 89.65 | 90.98 | 90.55 | 90.64 | 89.48 | 88.98 | 89.76 | 89.57 | 89.75 | 89.58 | 92.50 |
| ICV | 0.62 | 0.62 | 0.63 | 0.67 | 0.62 | 0.59 | 0.52 | 0.62 | 0.61 | 0.62 | 0.63 | 0.94 |
| SiO2/Al2O3 | 10.28 | 24.33 | 7.29 | 8.30 | 7.67 | 9.32 | 9.34 | 8.51 | 8.49 | 9.03 | 9.76 | 14.54 |
| $K_2O/Na_2O$ | 1.68 | 1.14 | 1.65 | 1.49 | 1.48 | 1.14 | 1.00 | 1.19 | 1.15 | 1.23 | 1.17 | 3.83 |
| $K_2O/Al_2O_3$ | 0.16 | 0.13 | 0.16 | 0.15 | 0.15 | 0.13 | 0.12 | 0.13 | 0.13 | 0.14 | 0.13 | 0.22 |

(*continued on next page*)

(*continued*)

| Samples | P1P | P1R | P2U | P2A | P2S | P3A | P3B | P3C | P3D | P3E | P3F | P3K |
|---|---|---|---|---|---|---|---|---|---|---|---|---|
| $Al_2O_3/TiO_2$ | 32.84 | 29.31 | 28.21 | 25.31 | 28.51 | 32.21 | 33.48 | 23.51 | 29.39 | 26.51 | 24.11 | 25.17 |
| **Trace elements(ppm)** | | | | | | | | | | | | |
| V | 49.00 | 20.00 | 64.00 | 63.00 | 62.00 | 48.00 | 45.00 | 59.00 | 48.00 | 55.00 | 52.00 | 64.00 |
| Cr | 60.00 | 60.00 | 60.00 | 100.00 | 60.00 | 60.00 | 70.00 | 70.00 | 60.00 | 70.00 | 70.00 | 60.00 |
| Co | 3.00 | 5.00 | 7.00 | 5.00 | 5.00 | 12.00 | 5.00 | 9.00 | 10.00 | 19.00 | 7.00 | 7.00 |
| Ni | 7.00 | 9.00 | 9.00 | 11.00 | 9.00 | 21.00 | 14.00 | 24.00 | 19.00 | 27.00 | 16.00 | 13.00 |
| Cu | 1.00 | 1.00 | 3.00 | 5.00 | 3.00 | 1.00 | 1.00 | 3.00 | 1.00 | 2.00 | 1.00 | 2.00 |
| Rb | 43.00 | 15.40 | 55.20 | 48.60 | 49.60 | 38.10 | 36.00 | 42.70 | 37.80 | 41.60 | 37.30 | 43.30 |
| Sr | 179.50 | 108.50 | 234.00 | 245.00 | 236.00 | 256.00 | 262.00 | 289.00 | 258.00 | 265.00 | 249.00 | 79.70 |
| Cs | 1.63 | 0.61 | 2.10 | 1.92 | 1.89 | 1.61 | 1.58 | 1.67 | 1.52 | 1.80 | 1.59 | 1.67 |
| Ba | 566.00 | 213.00 | 631.00 | 641.00 | 579.00 | 507.00 | 443.00 | 613.00 | 479.00 | 550.00 | 523.00 | 406.00 |
| Y | 29.40 | 7.90 | 27.00 | 21.20 | 26.20 | 17.00 | 14.30 | 23.90 | 11.70 | 29.00 | 28.20 | 10.10 |
| Zr | 55.00 | 87.00 | 75.00 | 117.00 | 116.00 | 65.00 | 57.00 | 96.00 | 56.00 | 82.00 | 72.00 | 65.00 |
| Hf | 1.70 | 2.30 | 2.20 | 3.30 | 3.00 | 1.80 | 1.70 | 2.60 | 1.70 | 2.30 | 2.00 | 1.90 |
| Nb | 2.40 | 1.60 | 3.80 | 4.00 | 3.70 | 2.60 | 2.70 | 4.00 | 3.00 | 3.40 | 3.70 | 2.20 |
| Ta | 0.10 | <0.1 | 0.10 | 0.20 | 0.20 | <0.1 | 0.10 | 0.20 | 0.10 | 0.10 | 0.20 | <0.1 |
| Sc | 9.00 | 5.00 | 11.00 | 11.00 | 11.00 | 9.00 | 8.00 | 12.00 | 10.00 | 10.00 | 9.00 | 7.00 |
| Th | 2.92 | 1.68 | 3.29 | 4.29 | 3.46 | 2.15 | 2.44 | 3.40 | 2.76 | 3.39 | 3.79 | 2.68 |
| **REEs** | | | | | | | | | | | | |
| La | 30.40 | 9.90 | 28.10 | 31.00 | 32.80 | 20.30 | 21.50 | 44.10 | 24.90 | 31.40 | 45.80 | 7.10 |
| Ce | 71.20 | 26.90 | 54.00 | 74.70 | 69.80 | 43.30 | 47.10 | 91.90 | 51.80 | 66.20 | 93.30 | 15.00 |
| Pr | 7.90 | 2.44 | 6.52 | 7.73 | 7.92 | 5.60 | 5.52 | 11.35 | 6.50 | 8.80 | 11.50 | 1.62 |
| Nd | 30.80 | 9.10 | 25.50 | 30.50 | 32.40 | 23.30 | 21.70 | 45.50 | 26.60 | 34.70 | 46.40 | 6.50 |
| Sm | 5.86 | 1.83 | 5.16 | 5.45 | 5.99 | 4.48 | 3.99 | 8.49 | 4.71 | 6.64 | 8.99 | 1.31 |
| Eu | 1.57 | 0.45 | 1.44 | 1.37 | 1.66 | 1.08 | 1.05 | 2.33 | 1.21 | 1.75 | 2.19 | 0.38 |
| Gd | 4.81 | 1.46 | 5.05 | 4.64 | 5.40 | 3.94 | 3.29 | 7.07 | 3.72 | 5.85 | 7.41 | 1.39 |
| Tb | 0.78 | 0.25 | 0.80 | 0.66 | 0.78 | 0.54 | 0.48 | 0.95 | 0.46 | 0.89 | 0.98 | 0.24 |
| Dy | 4.92 | 1.53 | 4.50 | 3.84 | 4.52 | 2.94 | 2.67 | 5.12 | 2.34 | 4.98 | 5.06 | 1.60 |
| Ho | 1.09 | 0.32 | 0.96 | 0.78 | 0.92 | 0.62 | 0.54 | 0.97 | 0.45 | 1.04 | 1.02 | 0.35 |
| Er | 2.84 | 0.78 | 2.67 | 2.13 | 2.48 | 1.71 | 1.39 | 2.52 | 1.16 | 2.92 | 2.73 | 1.09 |
| Tm | 0.40 | 0.13 | 0.38 | 0.30 | 0.35 | 0.24 | 0.20 | 0.34 | 0.16 | 0.39 | 0.37 | 0.17 |
| Yb | 2.13 | 0.69 | 1.97 | 1.66 | 2.05 | 1.36 | 1.08 | 1.84 | 0.93 | 2.02 | 2.12 | 1.11 |
| Lu | 0.28 | 0.10 | 0.27 | 0.21 | 0.29 | 0.20 | 0.16 | 0.26 | 0.15 | 0.28 | 0.28 | 0.17 |
| La/Sc | 3.38 | 1.98 | 2.55 | 2.82 | 2.98 | 2.26 | 2.69 | 3.68 | 2.49 | 3.14 | 5.09 | 1.01 |
| Th/Co | 0.97 | 0.34 | 0.47 | 0.86 | 0.69 | 0.18 | 0.49 | 0.38 | 0.28 | 0.18 | 0.54 | 0.38 |
| Rb/Sr | 0.24 | 0.14 | 0.24 | 0.20 | 0.21 | 0.15 | 0.14 | 0.15 | 0.15 | 0.16 | 0.15 | 0.54 |
| Th/U | 2.45 | 1.14 | 2.33 | 1.32 | 2.15 | 1.68 | 1.64 | 1.77 | 1.94 | 2.23 | 2.22 | 3.62 |
| Th/Sc | 0.32 | 0.34 | 0.30 | 0.39 | 0.31 | 0.24 | 0.31 | 0.28 | 0.28 | 0.34 | 0.42 | 0.38 |
| Cr/Th | 20.55 | 35.71 | 18.24 | 23.31 | 17.34 | 27.91 | 28.69 | 20.59 | 21.74 | 20.65 | 18.47 | 22.39 |
| Zr/Sc | 6.11 | 17.40 | 6.82 | 10.64 | 10.55 | 7.22 | 7.13 | 8.00 | 5.60 | 8.20 | 8.00 | 9.29 |
| Th/Cr | 0.05 | 0.03 | 0.05 | 0.04 | 0.06 | 0.04 | 0.03 | 0.05 | 0.05 | 0.05 | 0.05 | 0.04 |
| Sm/Nd | 0.19 | 0.20 | 0.20 | 0.18 | 0.18 | 0.19 | 0.18 | 0.19 | 0.18 | 0.19 | 0.19 | 0.20 |
| Cr/Sc | 6.67 | 12.00 | 5.45 | 9.09 | 5.45 | 6.67 | 8.75 | 5.83 | 6.00 | 7.00 | 7.78 | 8.57 |
| **ΣREE** | **132.18** | **41.88** | **121.32** | **122.47** | **134.76** | **92.31** | **85.87** | **166.74** | **94.99** | **140.66** | **172.05** | **40.13** |
| LaN/YbN | 3.69 | 3.71 | 3.69 | 4.83 | 4.14 | 3.86 | 5.15 | 6.20 | 6.93 | 4.02 | 5.59 | 1.65 |
| LaN/SmN | 1.25 | 1.31 | 1.31 | 1.37 | 1.32 | 1.09 | 1.30 | 1.25 | 1.28 | 1.14 | 1.23 | 1.31 |
| GdN/YbN | 1.82 | 1.71 | 2.07 | 2.26 | 2.13 | 2.34 | 2.46 | 3.10 | 3.23 | 2.34 | 2.82 | 1.01 |
| Eu/Eu* | 0.90 | 0.84 | 0.86 | 0.83 | 0.89 | 0.79 | 0.89 | 0.92 | 0.88 | 0.86 | 0.82 | 0.86 |

**CIA** = $[Al_2O_3/(Al_2O_3 + CaO^* + Na_2O + K_2O)] \times 100$,
**PIA** = $[(Al_2O_3K_2O)/(Al_2O_3+CaO^*+Na_2O - K_2O)]$ x100
**Eu/Eu*** = EuN/(SmN*GdN) $^{½}$, where **N** refers to normalized values.
**CIW** = $[Al_2O_3/(Al_2O_3+CaO^*+Na_2O)] \times 100$,
**ICV** = $[CaO + K_2O + Na_2O + Fe_2O_3$, (t) + MgO + MnO + $TiO_2]/Al_2O_3$
Normalizing values are from Boynton (1984).

## Data availability

Data will be made available on request.

## References


Abouchami, W., Boher, M., Michard, A., Albarede, F., 1990. A major 2.1 Ga event of mafic magmatism in West Africa. An early stage of crustal accretion. J. Geophys. Res. 95, 17605–17629.

Abu, M., Sunkari, E.D., 2020a. Geochemistry and petrography of beach sands along the western coast of Ghana: implications for provenance and tectonic settings. Turk. J. Earth Sci. 29 (2), 363–380.

Abu, M., Sunkari, E.D., 2020b. Geochemistry, grain size characterization and provenance of beach sands along the Central Coast of Ghana. Adv Res Chem Appl Sci 2, 15–26.

Adadey, K., Clarke, B., Théveniaut, H., Urien, P., Delor, C., Roig, J.Y., Feybesse, J.L., 2009. Geological Map Explanation-Map Sheet 0503 B (1:1 000 000), CGS/BRGM/Geoman. Geological Survey Department of Ghana (GSD). No MSSP/2005/GSD/5a.

Afify, A.M., Wanas, H.A., Osman, R.A., et al., 2023. Depositional environments, provenance, paleoclimate, and tectonic setting of the Paleozoic–Lower Mesozoic siliciclastic sedimentary rocks at Um Bogma region, southwestern Sinai, Egypt: facies analysis and geochemistry. Arabian J. Geosci. 16, 10. https://doi.org/10.1007/s12517-022-10979-6.

Agra, N.A., Elburg, M.A., Vorster, C., 2023. Constraints on paleoproterozoic crustal growth from birimian Supergroup lavas of the Bui belt (Ghana) in the West African craton. Precambrian Res. 384, 106926. https://doi.org/10.1016/j.precamres.2022.106926.

Akarish, A.I., El-Gohary, A.M., 2008. Petrography and geochemistry of lower Paleozoic sandstones, East Sinai, Egypt: implications for provenance and tectonic setting. J. Afr. Earth Sci. 52 (1–2), 43–54. https://doi.org/10.1016/j.jafrearsci.2008.04.002.

Amponsah, P.O., Kwayisi, D., Awunyo, E.K., Sapah, M.S., Sakyi, P.A., Su, B.X., Lu, Y., Nude, P.M., 2023. New evidence for crustal reworking and juvenile arc-magmatism during the Palaeoproterozoic Eburnean events in the Suhum Basin, South-east Ghana. Geol. J. 58 (10), 3734–3755.

Anani, C., 1999. Sandstone petrology and provenance of the neoproterozoic voltaian Group in the southeastern voltaian basin, Ghana. Sediment. Geol. 128 (1–2), 83–98.

Anani, C.Y., Mahamuda, A., Kwayisi, D., Asiedu, D.K., 2017. Provenance of sandstones from the neoproterozoic bombouaka Group of the volta basin, northeastern Ghana. Arabian J. Geosci. 10 (21). https://doi.org/10.1007/s12517-017-3243-2.

Anani, C.Y., Anim, R.O., Armah, B.N., Atichogbe, J.F., Sakyi, P.A., Mahu, E., Asiedu, D. K., 2020. Petrography of detrital zircons from sandstones of the lower devonian accraian formation, SE Ghana: implications on provenance. Geol. J. 55 (5), 3716–3731.

Anum, S., Sakyi, P.A., Su, B.-X., Nude, P.M., Nyame, F., Asiedu, D., Kwayisi, D., 2015. Geochemistry and geochronology of granitoids in the Kibi-Asamankese area of the Kibi-Winneba volcanic belt, southern Ghana. J. Afr. Earth Sci. 102, 166–179.

Armstrong-Altrin, J.S., Machain-Castillo, M.L., Rosales-Hoz, L., Carranza-Edwards, A., Sanchez-Cabeza, J.A., Ruíz-Fernández, A.C., 2015. Provenance and depositional history of continental slope sediments in the Southwestern Gulf of Mexico unraveled by geochemical analysis. Continent. Shelf Res. 95, 15–26. https://doi.org/10.1016/j.csr.2015.01.003.

Armstrong-Altrin, J.S., Lee, Y.I., Kasper-Zubillaga, J.J., Trejo-Ramirez, E., 2017. Mineralogy and geochemistry of sands along the Manzanillo and El Carrizal beach areas, southern Mexico: implications for palaeoweathering, provenance and tectonic setting. Geol. J. 52 (4), 559–582.

Asiedu, D., Dampare, S., Sakyi, P., Banoeng-Yakubo, B., Osae, S., Nyarko, B.J.B., et al., 2004. Geochemistry of Paleoproterozoic metasedimentary rocks from the Birim diamondiferous field, southern Ghana: implications for provenance and crustal evolution at the Archean-Proterozoic boundary. Geochem. J. 38. https://doi.org/10.2343/geochemj.38.215, 2004.

Armstrong-Altrin, J.S., Ramos-Vázquez, M.A., Zavala-León, A.C., Montiel-García, P.C., 2018. Provenance discrimination between Atasta and Alvarado beach sands, western Gulf of Mexico, Mexico: constraints from detrital zircon chemistry and U–Pb geochronology. Geol. J. 53 (6), 2901–2915. https://doi.org/10.1002/gj.3984.

Asiedu, D.K., Agoe, M., Amponsah, P.O., Nude, P.M., Anani, C.Y., 2019. Geochemical constraints on provenance and source area weathering of metasedimentary rocks from the Paleoproterozoic (~ 2.1 Ga) Wa-Lawra Belt, southeastern margin of the West African Craton. Geodin. Acta 31 (1), 27–39.

Asjad, S., Ahmad, A.H.M., Quasim, M.A., Sachan, H.K., 2021. Provenance, palaeoweathering and tectonic setting of the kuldhar member shale (Callovian–Oxfordian), jaisalmer formation, western Rajasthan. Journal of Sedimentary Environments 6, 585–602.

Atanga, F., Amponsah, P.O., Nunoo, S., Kwayisi, D., Forson, E.D., Akabzaa, T.M., Nude, P.M., 2023. The geology and geochemistry of the Rhyacian Josephine gold deposit, Northwest Ghana. B. Appl. Earth Sci.: Trans. Inst. Min. Metall. 132 (3–4), 252–270. https://doi.org/10.1080/25726838.2023.2260583.

Basu, A., Young, S.W., Suttner, L.J., James, W.C., Mack, G.H., 1975. Re-evaluation of the use of undulatory extinction and polycrystallinity in detrital quartz for provenance interpretation. J. Sediment. Petrol. 45, 873–882.

Berge, J., 2011. Paleoproterozoic, turbidite-hosted, gold deposits of the Ashanti gold belt (Ghana, West Africa): comparative analysis of turbidite-hosted gold deposits and an updated genetic model. Ore Geol. Rev. 39 (1–2), 91–100.

Bhatia, M.R., 1983. Plate tectonics and geochemical composition of sandstones. J. Geol. 91 (6), 611–627.

Bhatia, M.R., Crook, K.A.W., 1986. Trace elements characteristics of graywackes and tectonic Setting discrimination of sedimentary basins. Contrib. Mineral. Petrol. 92 (2), 181–193. https://doi.org/10.1007/BF00375292.

Boher, M., Abouchami, W., Michard, A., Albarede, F., Arndt, N.T., 1992. Crustal growth in West Africa at 2.1 Ga. J. Geophys. Res. Solid Earth 97 (B1), 345–369.

Boynton, W.V., 1984. Geochemistry of Rare Earth Elements: Meteorite Studies. In: Henderson, P. (Ed.), Rare Earth Element Geochemistry. Elsevier, New York, pp. 63–114. https://doi.org/10.1016/B978-0-444-42148-7.50008-3.

Brako, B.A., Amadu, C.C., Foli, G., Nude, P.M., Gawu, S.K.Y., 2022. Petrography and geochemistry of metasedimentary rocks from the Paleoproterozoic Birimian at the Chagupana area, North-West Ghana: implications for provenance and tectonic setting. Arabian J. Geosci. 15 (24). https://doi.org/10.1007/s12517-022-11036-y.

Carney, J.N., Jordan, J.L., Kalsbeek, F., 2010. Geology of the Nasia Basin, Northern Ghana: stratigraphy, structure, and tectonic evolution. Precamb. Res. 183 (1–2), 1–19. https://doi.org/10.1016/j.precamres.2010.07.001.

Chudasama, B., Porwal, A., Kreuzer, O.P., Butera, K., 2016. Geology, geodynamics and orogenic gold prospectivity modeling of the paleoproterozoic kumasi basin, Ghana, West Africa. Ore Geol. Rev. 78, 692–711.

Condie, K.C., 1989. Geochemical changes in basalts and andesites across the Archean-Proterozoic boundary: identification and significance. Lithos 23 (1–2), 1–18.

Condie, K.C., Boryta, M.D., Liu, J., Quian, X., 1992. The origin of chondrites: geochemical evidence from the archean to early proterozoic granulitic belt in the north China craton. Precambrian Res. 59 (1992), 207–223. Crystalline source rocks. Journal of Sedimentary Petrology, pp.46: 595–603.

Cox, R., Lowe, D.R., Cullers, R., 1995. The influence of sediment recycling and basement composition on the evolution of mudrock chemistry in the southwestern United States. Geochem. Cosmochim. Acta 59 (14), 2919–2940. https://doi.org/10.1016/0016-7037(95)00185-9.

Critelli, S., Arribas, J., Le Pera, E., Tortosa, A., Marsaglia, K.M., Latter, K.K., 2003. The Recycled Orogenic Sand Provenance from an Uplifted Thrust Belt, Betic Cordillera.

Cullers, R.L., 1988. Mineralogical and chemical changes of soil and stream sediment formed by intense weathering of the Danberg Granite, Georgia, USA. Lithos 21 (4), 301–314. https://doi.org/10.1016/0024-4937(88)90035-7.

Cullers, R.L., 1994. The controls on the major and trace element evolution of shales, siltstones, and sandstones of Ordovician to Tertiary age in the Wet Mountains region, Colorado, USA. Chem. Geol. 123 (1–4), 107–131.

Cullers, R.L., 2000. The geochemistry of shales, siltstones and sandstones of Pennsylvanian-Permian age, Colorado, USA: implications for provenance and metamorphic studies. Lithos 51 (3), 181–203.

Cullers, R.L., Podkovyrov, V.N., 2000. Geochemistry of the mesoproterozoic Lakhanda shales in Southeastern Yakutia, Russia: implications for mineralogical and provenance control, and recycling. Precamb. Res. 104 (1–2), 77–93. https://doi.org/10.1016/S0301-9268(00)00090-5.

Dampare, S., Shibata, T., Asiedu, D., Okano, O., Manu, J., Sakyi, P., 2009. Sr–Nd isotopic compositions of Paleoproterozoic metavolcanic rocks from the southern Ashanti volcanic belt, Ghana. Okayama Univ. Earth Sci. Rep. 16 (1), 9–28.

Davis, P.A., Breed, C.S., McCauley, J.F., Schaber, G.G., 1993. Surficial geology of the Safsaf region, south-central Egypt, derived from remote-sensing and field data. Rem. Sens. Environ. 46 (2), 183–203.

Davis, D.W., Hirdes, W., Schaltegger, E., Nunoo, E.A., 1994. U-Pb age constraints on deposition and provenance of Birimian and gold-bearing Tarkwaian sediments in Ghana, West Africa. Precambrian Res. 67, 89, 107. 4.

Dickinson, W.R., 1970. Interpreting detrital modes of greywacke and arkose. J. Sediment. Petrol. 40p, 605–707.

Dickinson, W.R., Suczek, C.A., 1979. Plate tectonics and sandstone composition. AAPG (Am. Assoc. Pet. Geol.) Bull. 63, 2164–2182.

Dickinson, W.R., 1985. Interpreting Provenance Relations from Detrital Modes of Sandstones. In: Zuffa, G.G. (Ed.), Provenance of Arenites, NATO ASI Series, 148. Springer, Dordrecht. https://doi.org/10.1007/978-94-017-2809-6_15.

Dickinson, W.R., Beard, L.S., Brakenridge, G.R., Erjavec, J.L., Ferguson, R.C., Inman, K.F., et al., 1983. Provenance of North American Phanerozoic sandstones in relation to tectonic setting. Geol. Soc. Am. Bull. 94 (2), 222–235.

Du Toit, R., 1996. Phase 1 Drilling proposal: Stratigraphic and Outline boreholes on Noyem and Sakapea Grids. Ghana Regional Office, Filling Reference Bulletin. Addendum 4.

Dutta, P.K., Suttner, L.J., 1986. Alluvial sandstone composition and paleoclimate; II, Authigenic mineralogy. J. Sediment. Res. 56 (3), 346–358.

Elzien, S.M., Farah, A.A., Alhaj, A.B., Mohamed, A.A., Al-Imam, O.A.O., Hussein, A.H., et al., 2014. Geochemistry of merkhiyat sandstones, omdurman formation, Sudan: implication of depositional environment, provenance and tectonic setting. International Journal of Geology, Agriculture and Environmental Sciences 2 (3), 10–15.

Fedo, C.M., Nesbitt, H.W., Young, G.M., 1995. Unraveling the effects of potassium metasomatism in sedimentary rocks and paleosols, with implications for paleoweathering conditions and provenance. Geology 23, 921–924.

Fedo, C.M., Eriksson, K.A., Krogstad, E.J., 1996. Geochemistry of shales from the archean (~3.0 Ga) buhwa greenstone belt, Zimbabwe: implications for provenance and source-area weathering. Geochem. Cosmochim. Acta 60 (10), 1751–1763. https://doi.org/10.1016/0016-7037(96)00058-0.

Fisher, W.S., 2019. Zircon facies in the paleocene-eocene orca Group indicate a provenance link to the chugach terrance, prince william sound, Alaska. In: Proceedings of the Keck Geology Consortium, 32.

Floyd, P.A., Leveridge, B.E., 1987. The tectonic environment of the Devonian Gramscatho basin, south Cornwall: framework mode and geochemical evidence from turbidite sandstones. Journal of the Geological Society of London 144, 531–542.

Garzanti, E., 2017. The maturity myth in sedimentology and provenance analysis. J. Sediment. Res. 87 (4), 353–365.

Garzanti, E., 2019. Petrographic classification of sand and sandstone. Earth Sci. Rev. 192, 545–563.

Garzanti, E., Andò, S., 2018. Sedimentary petrology: methods and applications. J. Sediment. Res. 88 (12), 1345–1362.

Ghaznavi, A.A., Khan, I., Quasim, M.A., Ahmad, A.H.M., 2018. Provenance, tectonic setting, source weathering and palaeoenvironmental implications of Middle-Upper Jurassic rocks of Ler dome, Kachchh, western India: inferences from petrography and geochemistry. Geochemistry 78 (3), 356–371.

Girty, G.H., Ridge, D.L., Knaack, C., Johnson, D., Al-Riyami, R.K., 1996. Provenance and depositional setting of Paleozoic chert and argillite, Sierra Nevada, California. J. Sediment. Res. 66 (1), 107–118.

Griffis, R.J., Barning, K., Agezo, F.L., Akosah, F.K., 2002. Gold Deposits of Ghana. Ghana: Minerals Commission, Accra, p. 438.

Hadji, F., Marok, A., Samet, A.M., et al., 2024. Inorganic geochemistry of Miocene sediments from the Lower Chelif Basin (NW Algeria) for approaching weathering and palaeoclimatic conditions. J. Iber. Geol. https://doi.org/10.1007/s41513-024-00236-y.

Harnois, L., 1988. The CIW index: a new chemical index of weathering. Sediment. Geol. 55 (3), 319–322.

Hayashi, K.I., Fujisawa, H., Holland, H.D., Ohmoto, H., 1997. Geochemistry of ~ 1.9 Ga sedimentary rocks from northeastern Labrador, Canada. Geochem. Cosmochim. Acta 61 (19), 4115–4137.

Herron, M.M., 1988. Geochemical classification of terrigenous sands and shales from core or log data. J. Sediment. Petrol. 58, 820–829.

Hirdes, W., Davis, D.W., Eisenlohr, B.N., 1992. Reassessment of Proterozoic granitoid ages in Ghana on the basis of U/Pb zircon and monazite dating. Precambrian Res. 56 (1–2), 89–96.

Hirdes, W., Davis, D., Ludtke, G., Konan, G., 1996. Two generations of Birimian (Paleoproterozoic) volcanic belts in northeastern Côte d'Ivoire (West Africa): consequences for the Birimian controversy. Precambrian Res. 80 (3–4), 173–191. https://doi.org/10.1016/s0301-9268(96)00011-3.

Huang, H., Huyskens, M.H., Yin, Q.Z., Cawood, P.A., Hou, M., Yang, J., et al., 2022. Eruptive tempo of Emeishan large igneous province, southwestern China and northern Vietnam: relations to biotic crises and paleoclimate changes around the Guadalupian-Lopingian boundary. Geology 50 (9), 1083–1087.

Ingersoll, R.V., Bullard, T.F., Ford, R.L., Grimm, J.P., Pickle, J.D., Sares, S.W., 1984. The effect of grain size on detrital modes: a test of the Gazzi-Dickinson point-counting method. J. Sediment. Petrol. 46, 620–632.

Jiang, G., Hu, S., Shi, Y., Zhang, C., Wang, Z., Hu, D., 2019. Terrestrial heat flow of continental China: updated dataset and tectonic implications. Tectonophysics 753, 36–48.

Johnsson, M.J., 1993. The system controlling the composition of clastic sediments. Geol. Soc. Am. Spec. Pap. 284, 1–20.
Kazapoe, R.W., Okunlola, O., Arhin, E., Olisa, O., Kwayisi, D., Dzikunoo, E.A., Amuah, E. E.Y., 2023. Compositional characteristics of mineralised and unmineralised gneisses and schist around the Abansuoso area, southwestern Ghana. B. Appl. Earth Sci. 132 (1), 36–51.
Kesse, G.O., 1985. The Mineral and Rock Resources of Ghana: A. A Balkema, Rotterdam, p. 610.
Klemd, R., Hunken, U., Olesch, M., 2002. Metamorphism of the country rocks hosting gold–gold-sulfide-bearing quartz veins in the Paleoproterozoic southern Kibi-Winneba belt (SE-Ghana). J. Afr. Earth Sci. 35 (2), 199–211.
Koffi, Y.H., Wenmenga, U., Djro, S.C., 2016. Tarkwaian deposits of the birimian belt of houndé: petrological, structural and geochemical study (Burkina-Faso, West Africa). Int. J. Geosci. 7, 685–700. https://doi.org/10.4236/ijg.2016.75053.
Kroonenberg, S.B., 1994. Effects of provenance, sorting, and weathering on the geochemistry of fluvial sands from different tectonic and climatic environments. Proceedings of the 29th international geological congress, Part A 69, 81.
Kwayisi, D., Lehmann, J., Elburg, M., 2022. Provenance and depositional setting of the Buem structural unit (Ghana): implications for the paleogeographic reconstruction of the West African and Amazonian cratons in Rodinia. Gondwana Res. 109, 183–204.
Leaders, F.T., Lipson, R., Kudzawu-D'Pherdd, R., 2018. Gold Deposits of the Birimian and Tarkwaian in Ghana.
Leube, A., Hirdes, W., 1986. The Birimian Supergroup of Ghana Depositional Environment, Structural Development, and Conceptual Model of an Early Proterozoic Suite, p. 260. Republican Number, 99 529, Archives B G R, Hannover.
Leube, A., Hirdes, W., Mauer, R., Kesse, G.O., 1990. The early Proterozoic Birimian Supergroup of Ghana and some aspects of its associated gold mineralization. Precambrian Research, 46, 139–165.
Li, H.B., Jia, D., Wu, L., Zhang, Y., Yin, H.W., Wei, G.Q., Li, B.L., 2013. Detrital zircon provenance of the Lower Yangtze foreland basin deposits: constraints on the evolution of the early Palaeozoic Wuyi–Yunkai orogenic belt in South China. Geol. Mag. 150 (6), 959–974.
Makulana, M., Baiyegunhi, C., Masango, S., 2022. Petrography, modal composition, and tectonic provenance of some selected sandstones from the Swaershoek and Alma Formations (Waterberg Group) and Glentig Formation, Limpopo Province, South Africa: evidence from framework grains. Arabian J. Geosci. 15, 697. https://doi.org/10.1007/s12517-022-09989-1.
Marsaglia, K.M., Barone, M., Critelli, S., Busby, C., Fackler-Adams, B., 2016. Petrography of volcaniclastic rocks in intra-arc volcano-bounded to fault-bounded basins of the Rosario segment of the Lower Cretaceous Alisitos oceanic arc, Baja California, Mexico. Sediment. Geol. 336, 138–146.
Maynard, R. Valloni, Yu, Hongzhou, 1982. Composition of modern deep-sea sands from arc-related basins. Geological Society Special… Geology. https://doi.org/10.1144/GSL.SP.1982.010.01.36. Corpus ID: 128401710.
McLennan, S.M., Taylor, S.R., 1991. Sedimentary rocks and crustal evolution: tectonic setting and secular trends. J. Geol. 99 (1), 1–21.
McLennan, S.M., Taylor, S.R., McCulloch, M.T., Maynard, J.B., 1990. Geochemical and Nd–Sr isotopic composition of deep-sea turbidites: crustal evolution and plate tectonic associations. Geochem. Cosmochim. Acta 54, 2015–2050.
McLennan, S.M., Hemming, S., McDaniel, D.K., Hanson, G.N., 1993. Geochemical approaches to sedimentation, provenance, and tectonics. In: Johnson, M.J., Basu, A. (Eds.), Processes Controlling the Composition.
Morton, A.C., Hallsworth, C., 1994. Identifying provenance-specific features of detrital heavy mineral assemblages in sandstones. Sediment. Geol. 90 (3–4), 241–256.
Nagarajan, R., Armstrong-Altrin, J.S., Nagendra, R., Madhavaraju, J., Moutte, J., 2007. Petrography and geochemistry of terrigenous sedimentary rocks in the Neoproterozoic Rabanpalli Formation, Bhima Basin, Southern India: implications for paleoweathering conditions, provenance and source rock composition. J. Geol. Soc. India 70 (2), 297.
Nesbitt, R.W., Young, G.M., 1982. Early Proterozoic climates and plate motions inferred from major elements chemistry of lutites. Nature 29, 715–717.
Nesbitt, H.W., Young, G.M., 1984. Prediction of some weathering trends of plutonic and volcanic rocks based on thermodynamic and kinetic considerations. Geochem. Cosmochim. Acta 48 (7), 1523–1534.
Nesbitt, H.W., Markovics, G., Price, R.C., 1980. Chemical processes affecting alkalis and alkaline earths during continental weathering. Geochem. Cosmochim. Acta 44, 1659–1666.
Nesbitt, H.W., Young, G.M., 1989. Formation and diagenesis of weathering profiles. J. Geol. 97 (2), 129–147.
Nunoo, S., Hofmann, A., Kramers, J., 2022. Geology, zircon U–Pb dating and εHf data for the Julie greenstone belt and associated rocks in NW Ghana: implications for Birimian-to-Tarkwaian correlation and crustal evolution. J. Afr. Earth Sci. 186, 104444.
Oberthür, T., Weiser, T., Amanor, J.A., Chryssoulis, S.L., 1997. Mineralogical siting and distribution of gold in quartz veins and sulfide ores of the Ashanti mine and other deposits in the Ashanti belt of Ghana: genetic implications. Miner. Deposita 32, 2–15.
Panahi, A., Young, G.M., 1997. A geochemical investigation into the provenance of the neoproterozoic port askaig tillite, dalradian Supergroup, western scotland. Precambrian Res. 85 (1–2), 81–96.
Perrouty, S., Aillères, L., Jessell, M.W., Baratoux, L., Bourassa, Y., Crawford, B., 2012. Revised Eburnean geodynamic evolution of the gold-rich southern Ashanti Belt, Ghana, with new field and geophysical evidence of pre-Tarkwaian deformations. Precambrian Res. 204, 12–39.
Pettijohn, F.J., Potter, P.E., Siever, R., 1987. Sand and Sandstone. Springer Verlag, New York, p. 553.
Pigois, J.P., Groves, D.I., Fletcher, I.R., McNaughton, N.J., Snee, L.W., 2003. Age constraints on Tarkwaian palaeoplacer and lode-gold formation in the Tarkwa-Damang district, SW Ghana. Miner. Deposita 38, 695–714.
Plank, T., Langmuir, C.H., 1998. The chemical composition of subducting sediment and its consequences for the crust and mantle. Chem. Geol. 145 (3–4), 325–394. https://doi.org/10.1016/j.chemgeo.2014.07.022.
Potter, P.E., Maynard, J.B., Depetris, P.J., 2005. Mud and mudstones: Introduction and overview. Springer Science & Business Media.
Roddaz, M., Debat, P., Nikiéma, S., 2007. Geochemistry of Upper Birimian sediments (major and trace elements and Nd–Sr isotopes) and implications for weathering and tectonic setting of the Late Paleoproterozoic crust. Precambrian Res. 159 (3–4), 197–211.
Rollinson, H.R., 1993. Using Geochemical Data: Evaluation, Presentation, Interpretation. Longman, New York, USA, p. 352.
Roser, B.P., Korsch, R.J., 1986. Determination of tectonic setting of sandstone mud suite using $SiO_2$ content and $K_2O/Na_2O$ ratio. J. Geol. 94, 635–650.
Sakyi, P.A., Su, B.X., Anum, S., Kwayisi, D., Dampare, S.B., Anani, C.Y., Nude, P.M., 2014. New zircon U–Pb ages for erratic emplacement of 2213–2130 Ma paleoproterozoic calc-alkaline I-type granitoid rocks in the lawra volcanic belt of northwestern Ghana, West Africa. Precambrian Res. 254, 149–168.
Sakyi, P.A., Manu, J., Su, B.X., Kwayisi, D., Nude, P.M., Dampare, S.B., 2019. Geochemical and Sm–Nd isotopic evidence for the composition of the palaeoproterozoic crust of the West African craton in Ghana. Geol. J. 54 (6), 3940–3957. https://doi.org/10.1016/j.precamres.2019.105492 ecambrian Research, 336, 105492.
Sakyi, P.A., Addae, R.A., Su, B.X., Dampare, S.B., Abitty, E., Su, B.C., Liu, B., Asiedu, D. K., 2020. Petrology and geochemistry of TTG and K-rich paleoproterozoic birimian granitoids of the West African craton (Ghana). Petrogenesis and Tectonic Implications.
Sen, S., Mishra, M., 2023. Implications of heavy mineral assemblage to sediment recycling, rare earth element budget and provenance of Kaimur sandstones, Vindhyan Supergroup, Son Valley. J. Earth Syst. Sci. 132 (1), 5.
Sestini, G., 1973. Sedimentology of a paleoplacer: the gold-bearning tarkwaian of Ghana. In: Ores in Sediments: VIII. International Sedimentological Congress, Heidelberg, August 31–September 3, 1971. Springer Berlin Heidelberg, Berlin, Heidelberg, pp. 275–305.
Smith, A.J., Henry, G., Frost-Killian, S., 2016. A review of the birimian supergroup-and tarkwaian group-hosted gold deposits of Ghana. Episodes Journal of International Geoscience 39 (2), 177–197.
Sunkari, E.D., Oppong, O., Agbenyezi, T.K., 2024a. Petrogenetic and geochemical characteristics of some auriferous granitoids in the Kumasi Basin, Ghana: implications for geodynamic settings and controls of orogenic gold mineralization in the Edikan Gold Mine. Deep Underground Science and Engineering 1–16. https://doi.org/10.1002/dug2.12128.
Sunkari, E.D., Gan, A.N., Fiadonu, E.B., 2024b. Geochemical vectors for targeting hydrothermal gold mineralization in the Damang area, southwestern Ghana: constraints from petrography, multi-element geochemistry and multivariate statistical analysis. Ore and Energy Resource Geology 100071. https://doi.org/10.1016/j.oreoa.2024.100071.
Suttner, L.J., Dutta, P.K., 1986. Episodic tectonism and sedimentation in the upper proterozoic to lower cambrian windermere Supergroup, southeastern Canadian cordillera. Can. J. Earth Sci. 23 (4), 540–552.
Suttner, L.J., Basu, A., Mach, G.H., 1981. Climate and the origin of Quartz arenites. J. Sediment. Petrol. 51, 1235–1246.
Sylvester, P.J., Attoh, K., 1992. Lithostratigraphy and composition of 2.1 Ga greenstone belts of the West African Craton and their bearing on crustal evolution and the Archean-Proterozoic boundary. J. Geol. 100 (4), 377–393.
Taylor, R., Ikingura, J., Fallick, A., Huang, Y., Watkinson, D., 1992. Stable isotope compositions of tourmalines from granites and related hydrothermal rocks of the Karagwe-Ankolean belt, northwest Tanzania. Chem. Geol. Isot. Geosci. 94 (3), 215–227. https://doi.org/10.1016/0168-9622(92)90014-2.
Tortosa, A., Palomares, M., Arribas, J., 1991. Quartz grain types in Holocene deposits from the Spanish Central System: some problems in provenance analysis. In: Morton, A.C., Todd, S.P., Haughton, P.D.W. (Eds.), Developments in Sedimentary Provenance Studies, 57. Geological Society of London, Special Publication, pp. 47–54.
Verma, S.P., Armstrong-Altrin, J.S., 2013. New multi-dimensional diagrams for tectonic discrimination of siliciclastic sediments and their application to Precambrian basins. Chem. Geol. 355, 117–133.
Verma, S.P., Armstrong-Altrin, J.S., 2016. Geochemical discrimination of siliciclastic sediments from active and passive margin settings. Sediment. Geol. 332, 1–12.
Weaver, P.P.E., Thompson, J., Jarvis, I., 1989. The geology and geochemistry of Madeira Abyssal Plain sediments: a review. In: SUT Disposal of Radioactive Waste in Seabed Sediments: Proceedings of an International Conference. SUT-AUTOE). SUT.
Weltje, G.J., 1994. Provenance and Dispersal of Sand-Sized Sediment: Reconstruction of Dispersal Patterns and Sources of Sand-Sized Sediments by Means of Inverse Modelling Techniques.

Weltje, G.J., von Eynatten, H., 2004. Quantitative provenance analysis of sediments: review and outlook. Sediment. Geol. 171 (1–4), 1–11.
Wilson, M.C., Amedjoe, G.C., Gawu, S.K.Y., 2022. Petrographic and geochemical constraints on tectonic settings of the birimian Supergroup volcanic rocks, evidence from new drobo environs south of jaman district in the bono region of Ghana. Malaysian Journal of Geosciences (MJG) 6 (2), 73–83.
Yadav, P.K., Das, M., Ray, S., 2022. Geology, petrology, and geochemistry of the Mesoproterozoic Kaimur Group of rocks of the Vindhyan Supergroup, Eastern India: implications for depositional environment and sequence stratigraphy. J. Sediment. Environ. 7, 443–469. https://doi.org/10.1007/s43217-022-00105-7.